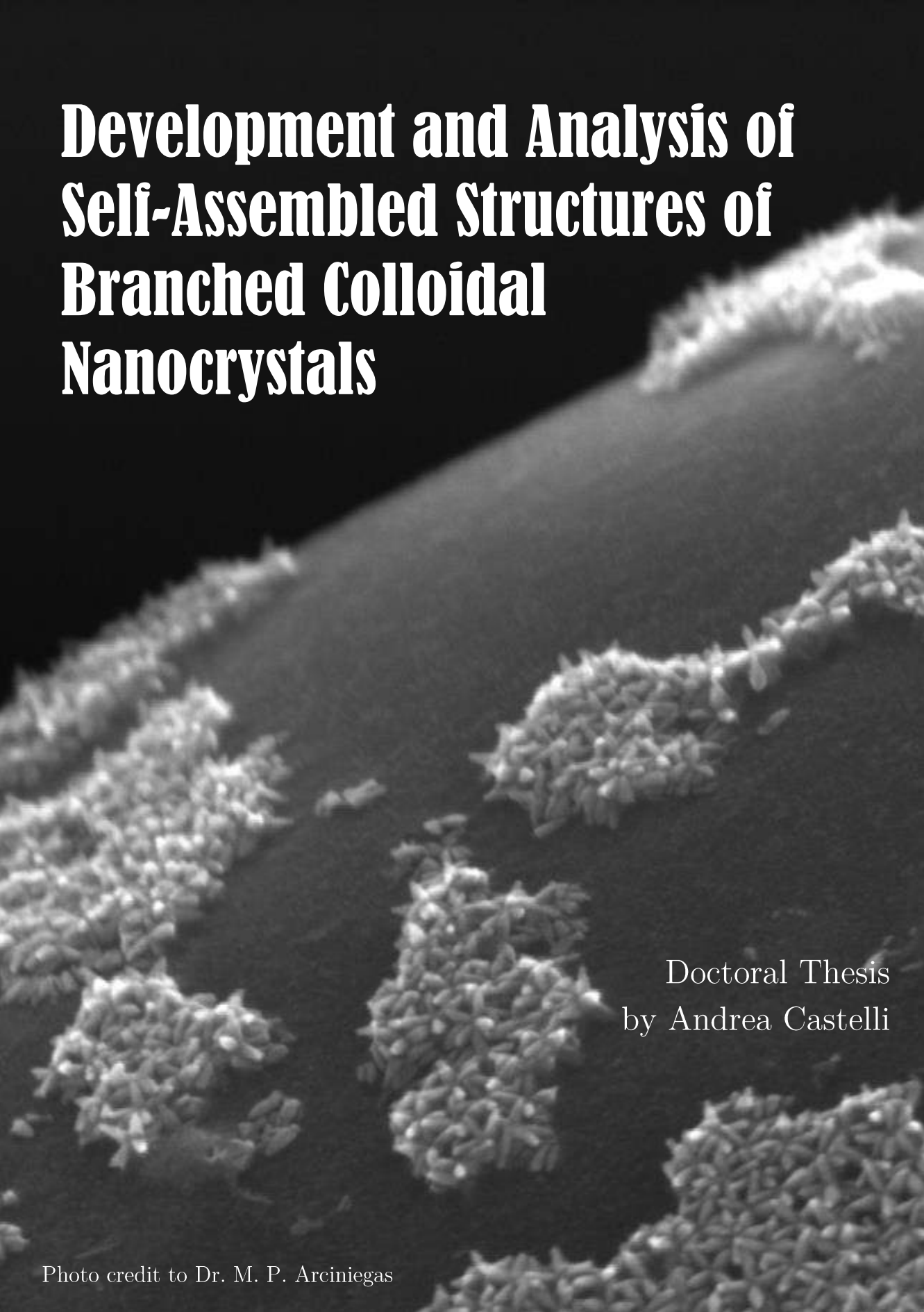


Development and Analysis of Self-Assembled Structures of Branched Colloidal Nanocrystals

A scanning electron micrograph (SEM) showing several branched, star-like structures of colloidal nanocrystals. The structures are composed of numerous small, spherical particles that have self-assembled into a central core with multiple arms extending outwards. The background is dark, and the structures are illuminated from the side, creating a sense of depth and highlighting their intricate, fractal-like geometry.

Doctoral Thesis
by Andrea Castelli

Nanochemistry Department,
Istituto Italiano di Tecnologia

Dipartimento di Chimica e Chimica Industriale
Università degli Studi di Genova

Development and Analysis of Self-Assembled Structures of Branched Colloidal Nanocrystals

Doctoral Thesis
by Andrea Castelli

Thesis submitted to attain the degree of Doctor of Philosophy in
Sciences and Technologies of Chemistry and Materials

Supervisors:

Prof. L Manna

Dr. M.P. Arciniegas

Prof. F. Buatier de Mongeot

Genova, Italy
December, 2017

The atmosphere was strange, the turmoil was growing, a weird, mechanically disquieting frenzy possessed everything. All were moving randomly, but somehow following the same vibe. Not all. He cannot feel that tune which was hypnotizing the others, forcing them to move, to speed up, swirling, hopping, crawling. A vortex of limbs, a chaos of arms hitting, punching, bouncing, kicking him as he always was on the wrong place. Then everything stopped, frozen. A cold light showed him the Order, the perfect alignment, the great assembly. He could admire it, scared and unwanted. He cannot join it, he was an insult to it.

He was defected.





Contents

Contents	7
1 Introduction	13
1.1 Synthesis of Colloidal Nanocrystals	15
1.2 Self-Assembly of Colloidal Nanocrystals	19
1.2.1. Driving Forces for the Self-Assembly of Nanocrystals.....	22
1.2.2. Strategies for th Self-Assembly of Colloidal Nanocrystals.....	28
1.3 Thesis Outline	30
1.4 References.....	33
2 Size Tuning and Surface Analysis of Branched Colloidal Nanocrystals	47
2.1 Synthesis and Characterization of Branched Colloidal Nanocrystals with different sizes.....	51



2.2	Surface Analysis of Branched Colloidal Nanocrystals with Different Sizes.....	60
2.3	Conclusions and Outlook.....	69
2.4	Acknowledgements	69
2.5	References.....	70
3	Planar Self-Assembly of Branched Colloidal Nanocrystals	75
3.1	Interfacial Self-Assembly Technique	77
3.2	Planar Self-Assembly of Native Octapods.....	78
3.3	Role of the Native Anisotropic Ligand Shell on the Self-Assembly of Octapods.....	84
3.4	Self-Assembly of Ligand-Exchanged Octapods.....	88
3.5	Conclusions and Outlook.....	97
3.6	Acknowledgements	98
3.7	References.....	98
4	Binary Self-Assembly of Branched Colloidal Nanocrystals	101
4.1	Planar Self-Assembled Structures of Octapods and Spheres via Shape-Complementary Interactions	104
4.2	3D Self-Assembled Structures of Octapods and Nanocubes via Attractive Surface Charges - Ongoing Project	119



4.2.1. 3D Self-Assembly of Octapods and Cubes from an Apolar Solvent	120
4.2.2. Modification of Surface Electrostatic Charges in Octapods	122
4.2.3. Self-Assembly Behaviour of Octapods with Different ζ -Potential.....	126
4.2.4. 3D Binary Self-Assembly of Octapods and Nanocubes via ζ -Potential Tuning	130
4.2.5. Strategies for Overcoming the Self-Assembly Issues.....	135
4.3 Conclusions and Outlook	137
4.4 Acknowledgements	139
4.5 References.....	139

5 Reinforced Nanocomposites: Self-Assembly of Branched Colloidal Nanocrystals in Polymer Films..... 143

5.1 Fabrication and Morphological Characterization of Self-Assembled Structures of Octapods in a Polymer Film	145
5.2 Effect of Polymer Viscosity on the Self-Assembly of Octapods in a Polymer Film.....	153
5.3 Fabrication of Free-standing Polymer Thick Films with Embedded Self-Assembled Structures of Octapods.....	157
5.4 Impact of Self-Assembled Structures of Octapods on the Mechanical Response of Polymer Films.....	161



5.5	Conclusions and Outlook.....	167
5.6	Acknowledgements	167
5.7	References.....	168
6	Synthesis and Self-Assembly of New Anisotropic Colloidal Nanocrystals - Ongoing Project.....	173
6.1	Synthesis and Morphological Characterization of Anisotropic Nanocrystals with Different Sizes.....	175
6.2	Structural and Optical Characterization of Bone-like Colloidal Nanocrystals.....	179
6.3	Planar Self-Assembly of Nanobones - Preliminary results	185
6.4	Conclusions and Outlook.....	188
6.5	Acknowledgements	189
6.6	References.....	189
	Appendix A: Details about the Cu_{2-x}Se Seeds Amount Employed in the Syntheses of Octapods	193
	Appendix B: Collection of Snapshots from the Monte Carlo Simulations of the Self-Assembly of Octapods into Planar Superlattices.....	195



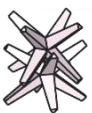
Appendix C: List of Chemicals..... 207

Appendix D: Characterization

Techniques	209
D.1 Transmission Electron Microscopy.....	210
D.1.1. General Transmission Electron Microscopy imaging.....	210
D.1.2. High Angle Annular Dark Field - Scanning TEM Imaging	210
D.2 Energy Dispersive X-Ray Spectroscopy	210
D.3 Electron Tomography of Colloidal Nanocrystals.....	211
D.4 High Resolution Scanning Electron Microscopy	211
D.5 X-ray Diffraction.....	211
D.6 Emission Spectroscopy	212
D.7 Absorption Spectroscopy.....	212
D.7.1. Fourier-Transform InfraRed Spectroscopy.....	212
D.7.2. Ultraviolet-Visible-Near Infrared Absorption Spectroscopy.....	212
D.8 Fluorescence Microscopy	213
D.9 Thermal Annealing of the Composites.....	213
D.10 Plasma Treatment of the Composites.....	213
D.11 Mechanical Tests on Composites	214
D.12 ζ -Potential Measurements	214



D.13 Inductively Coupled Plasma Optical Emission Spectroscopy	214
D.14 References.....	215
List of Scientific Contribution.....	217
Peer reviewed papers.....	218
Communications at Conferences	220
Personal Acknowledgements.....	221



1 Introduction

Materials science has been the foundation above which mankind has built its technology. Mastering the use of stone, copper, bronze and iron was so fundamental in human progress that entire ages were named after these materials. In the XX century, a new revolution took place: the introduction of polymeric and semiconductor materials. They opened the way to the realization of new devices, providing the flexibility and the optoelectronic features that empower nowadays technology. At the end of the century, a new branch of materials made its first promising steps: colloidal nanoparticles. These are objects with a controlled size in the range of 1-100 nm and defined shape, chemical composition, and structure¹.

They are dispersible in liquid media and typically produced by synthetic methods, which exploit the surface stabilization provided by organic surfactants, called ligands. These molecules are bound to the NCs surface to prevent their aggregation and confine their size in the nanoscale. Scientists refer to such particles also as nanocrystals (NCs), since they are usually formed by crystalline materials. Due to their peculiar optical and electrical properties, they are also labelled as “artificial atoms”². As atoms, indeed, NCs



can form crystalline solids, where their cooperative behaviour gives birth to collective properties³. The spontaneous formation of such ordered superstructures is known as NCs self-assembly⁴. While the geometry of atomic lattices mainly depends on the electronic configuration of their elements⁵, the arrangement of NCs in their self-assembled superlattices is primarily dictated by the shape of the single components and by attractive and repulsive interactions among them⁶. Interestingly, colloidal NCs with an anisotropic shape, provide access to a variety of self-assembled architectures^{7,8}. Branched NCs, in particular, are able to produce highly complex superlattices, in part thanks to their intrinsic convexity⁹⁻¹¹. Their intricate morphology, formed by different pods that grow from a common core, allows them also to host other components and form binary superlattices^{10,12,13}. Despite the fascinating arrangements that this class of NCs can form, their assembly has remained a challenge. This is mainly due to difficulties in effectively governing the combination of entropic arguments, short-range and long-range interactions that drives their organization.

In order to address these major points, the present thesis aims to elucidate how morphological engineering of branched NCs and control over their ligand shell can direct their assembly. In particular, we focus on the controlled fabrication of two- and three-dimensional (2D and 3D) superlattices, the development and analysis of binary ordered structures with isotropic and anisotropic NCs, and the fabrication of ordered assemblies in a polymer film. In this work, the organization of NCs will be directed acting on both the NC synthesis, to control size and shape, and on the interaction employed to guide their self-assembly, such as tuning of the ligand coating and use of different self-assembly experimental techniques. In this chapter, we describe the main concepts in which this thesis is based, from a brief description of the synthesis of colloidal NCs, to an overview of their self-assemblies, that includes prime driving forces and techniques so far implemented for their fabrication.



1.1 Synthesis of Colloidal Nanocrystals

In order to stabilize NCs in a solvent and prevent their aggregation, organic molecules that are able to be adsorbed on the facets of the NCs, are usually introduced in colloidal syntheses¹⁴. The high surface-to-volume ratio of the particles, indeed, provides to the system an elevated energy that would otherwise bring the NCs to coalescence.

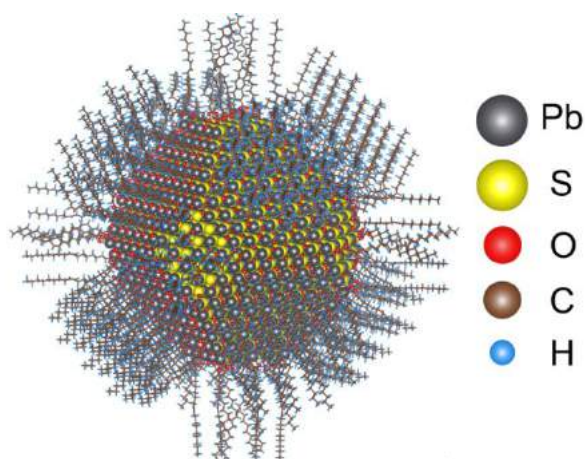


Figure 1. Atomistic model of a PbS colloidal NC stabilized by organic molecules (oleic acid) bound to its surface Image adapted from¹⁵.

The functions of ligands on the NCs surface are multiple: i) saturation of the dangling bonds at the inorganic surface; ii) steric prevention of the contact between the inorganic cores that could cause coalescence; and iii) promoting dispersibility of the NCs in the liquid media to form proper colloidal suspensions¹⁶. The overall aspect of a NC, as depicted in Figure 1, consists, thus, of an inorganic crystalline core coated by an organic ligand shell. This configuration is the most common and it describes the NCs employed in the present thesis. The concept of colloidal nanoparticle, however, is broader, as the core might be formed by polymer¹⁷ or glass¹⁸ and the shell can also consist of polymers¹⁹ or inorganic ions²⁰.



During the last two decades, several studies have been devoted to the nucleation and growth mechanisms of NCs^{21,22}. Monodispersed NCs, that follow the LaMer nucleation and growth mechanism²³, are usually obtained by separating the nucleation step from the growth via hot injection syntheses²⁴. This technique consists in a fast injection of precursors in a hot reaction environment, where they are transformed in reactive species (monomers). In this way, the concentration of monomers rises over the nucleation threshold only for a brief period of time. All the nuclei are thus formed together and grow homogeneously. The growth, then, occurs under reagents diffusion control, as the reactive species have to reach the crystalline surface passing through the ligands coating barrier^{16,21}. In order to have a narrow size distribution, the particle growth should be performed at high monomer concentration, since this allows the smaller particles to grow faster than the bigger ones²⁴. In this process, there are several parameters, such as reaction temperature²⁵, duration²⁶, reagents concentration²⁷ and ligand type²⁸, that can be controlled to tune the final size of the products. In the context of NCs self-assembly, obtaining monodisperse batches of particles is extremely important, since NCs with different sizes can act as defects and hinder the formation of long-range ordered structures.

On the other hand, when materials are produced with nanometric size, properties that are considered intensive in bulk (melting temperature, band gap, conductivity, among others) show a dependence on the NC dimension²⁹. Two key factors contribute to this: increased surface-to-volume ratio in the particles and quantum confinement. The abundance of surface atoms brings to a reduction of the bonding energy per single atom, increasing atomic mobility³⁰. This results, for example, in the coexistence of the solid and liquid phases over a wide range of temperatures or in the appearance of negative heat capacity³¹⁻³². Quantum confinement happens when at least one dimension of the NCs is smaller than the region explored in bulk by a charge carrier, limiting its delocalization and increasing



its kinetic energy³³. This brings to the formation of discrete energy states and the consequent modification of optical and electronic properties of the particle³⁴⁻³⁹. Several appealing properties derives from quantum confinement, such as, the Coulomb blockade effect, where only a single electron at a time can pass through the NC^{2,35,40}, or atomic-like sharp emission, whose colour dependence on NCs size found wide use in light emitting diodes (LEDs) and lasers⁴¹⁻⁴⁵.

As well as the size, the shape of the NCs plays an important role in their properties.^{37,46}. Indeed, producing particles with non-spherical shape allows to exploit functionalities deriving from the break of perfect isotropy. For example, the realization of nanoplatelets with 1D quantum confinement allows to exploit the peculiar emission properties of quantum wells (QW)⁴⁷, while the realization of elongated, rod-shaped shells around a QD induce the heterostructure to emit polarized light⁴⁶. In the field of metallic NCs the effect of the shape in enhancing the plasmonic resonance is extremely relevant⁴⁸.

The control of properties at nanoscale through tuning NC size and shape has motivated several investigations. Therefore, we have access nowadays to a wide library of NCs with different shapes and size, two fundamental parameters to direct their self-assemblies. (Figure 2)⁴⁹. Such morphologies of NCs are achieved via kinetic control of the particle growth during the synthesis. At low growth rate thermodynamic considerations dictates the shape of NCs, pointing toward spherical or quasi-spherical particles in order to minimize energy by exposing less surface⁵⁰⁻⁵³. At high growth rate, instead the growth of a single facet becomes exponentially dependant on its surface energy. This makes high energy facets to grow faster than low-energy and stable ones²⁴. Proper selection of ligands, moreover, helps to stabilize or destabilize a certain facet, actively sculpting the NCs⁵⁴.



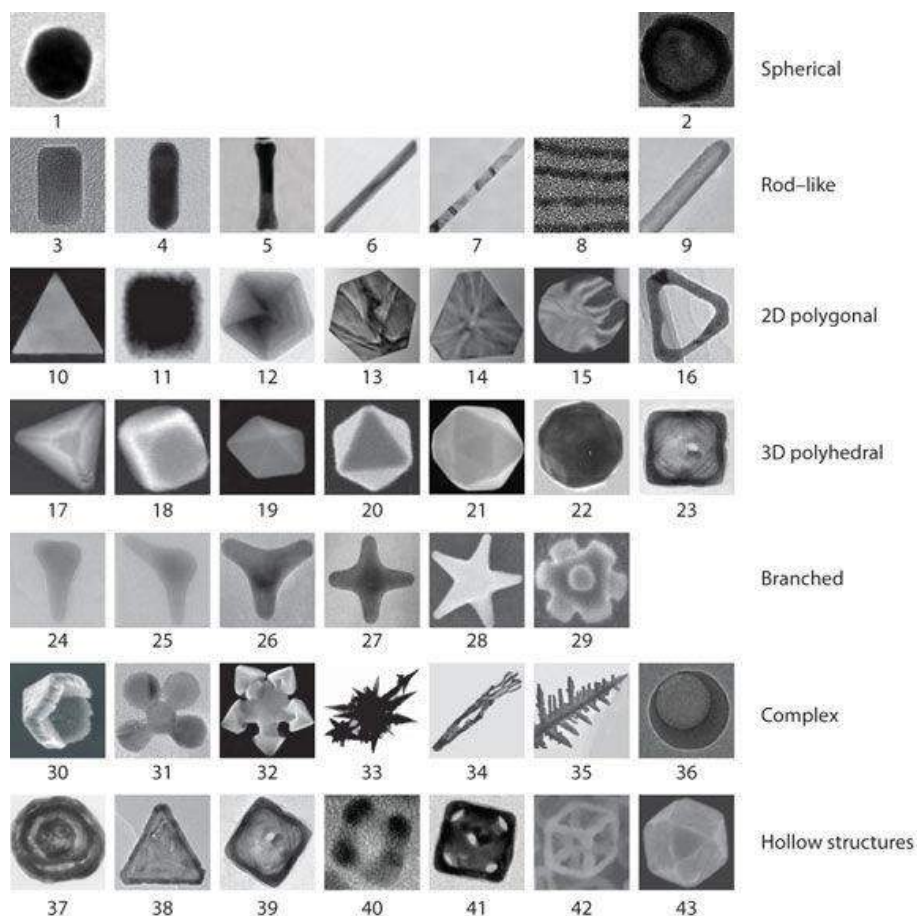


Figure 2. A “periodic table” of plasmonic NCs with different shapes: from spheres to 2D and 3D polyhedral geometries, and from particle with multiple branches to hollow nanostructures. Image adapted from [49].

Such morphologies of NCs are achieved via kinetic control of the particle growth during the synthesis. At low growth rate thermodynamic considerations dictates the shape of NCs, pointing toward spherical or quasi-spherical particles in order to minimize energy by exposing less surface⁵⁰⁻⁵³. At high growth rate, instead the growth of a single facet becomes exponentially dependant on its surface energy. This makes high energy facets to grow faster than low-energy and stable ones²⁴. Proper selection of ligands, moreover, helps to stabilize or destabilize a certain facet, actively sculpting



the NCs⁵⁴. Overall, this approach has been used in the last decade, to synthesize NCs made of a single material, directly synthesized from molecular or ionic precursors, as templating seeds in other synthesis processes⁵⁵, or undergo post-synthesis treatment, such as calcination⁵⁶ or cation/anion exchange^{57,58}. These multi-steps protocols have made possible to modify the composition of NCs, their structure, and shape. With these further modifications unusual geometries like, among others, QDs embedded in a rod⁵⁹, Au-FeO_x dumbbell heterodimers⁶⁰ or hollow particles⁶¹ have been reported.

In parallel, highly anisotropic NCs, such as particles with multiple branches, have been synthesized, when the kinetic growth regime is applied to a system that support polytypism⁶². This phenomenon consists in the growth of one phase of the material on another phase of the same material starting from a common facet. For example, CdSe pods with a hexagonal close packed (*hcp*) crystal structure can be grown on a core made of face centred cubic (*fcc*) CdSe by exploiting the equivalence between $(0001)_{hcp}$ and $(111)_{fcc}$ planes⁹.

The colloidal synthesis of NCs have been demonstrated to be a powerful and flexible tool, able to provide control over a wide spectrum of characteristics of the product. Particles made of metallic, semiconducting or insulating materials can be obtained with control over size, shape and crystalline structure. The availability of a wide variety of NCs has spurred the investigation of their properties, envisioning their application in several fields, from nanomedicine^{63,64} to optoelectronic^{65,66}, from catalysis^{67,68} to energy storage^{69,70}.

1.2 Self-Assembly of Colloidal Nanocrystals

The ability to control the shape and the size of NCs through their syntheses, has facilitated the studies on their self-assembly³,



which has resulted in the formation of a wide range of superlattices including unusual geometries, from honeycombs⁷¹ to interlocked linear arrays¹², from liquid crystals⁷² to intricate binary structures⁷³ (Figure 3).

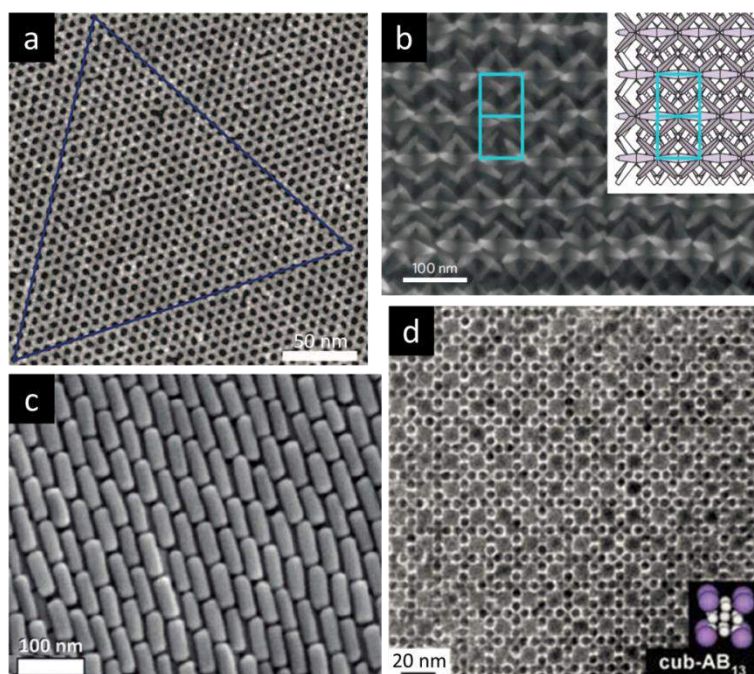


Figure 3. Examples of NCs self-assembly. (a) PbSe honeycomb superlattice formed by oriented attachment⁷⁴; (b) Ordered aggregation of chains made of interlocked branched colloidal NCs (octapods)⁷⁴; (c) Smectic organization of gold nanorods⁷¹; (d) Binary assembly of 6.2 nm PbSe and 3.0 nm Pd spherical particles⁷³.

These ordered structures showcase unique properties given by their nanometric periodicity. In analogy with atomic crystals superlattices of, for instance, QDs are expected to form delocalized electron states, allowing an excellent charge transport which is appealing for LEDs⁷⁵. However the ligand shells coating their surface prevent this phenomenon since it creates a potential thick barrier that results difficult to be tunnelled³. The exchange of ligands with compact, nucleophilic molecules has been envisioned as



a viable way to overcome this issue²⁰ but reliable self-assembly techniques have yet to be implemented for NCs showcasing such ligand shell³. In another example, the fabrication of devices emitting polarized light have been demonstrated by using self-assembled layers of dot-in-rods with aligned main axes⁷⁶. Another interesting property arising from the ordering of NCs is the plasmonic coupling between electromagnetic field and structures of metallic particles. Such coupling have proved to be sensitive toward the presence of local chirality in the organized array⁷⁷ and, in the case of binary superlattices, toward the NCs packing symmetry⁷⁸. These binary assemblies had been then effectively employed, for instance, in surface-enhanced Raman scattering (SERS) experiments⁷⁹. On the other hand, plasmonic photonic crystals had been realized with the use of superlattices made of DNA-coated metallic NCs⁸⁰.

The self-assembly of colloidal NCs allows also to mix components with different properties in ordered structures, giving rise to synergistic effects. For example, binary superlattices of semiconductor QDs and plasmonic NCs were proven to originate a non-radiative decay pathway for the excited electrons via energy transfer among particles⁸¹. Binary assemblies of magnetic NCs of different sizes (and thus different blocking temperatures), meanwhile, show a single blocking temperature, implying that the magnetic moments of the smaller NCs are pinned to those of the larger ones, an effect appealing for magnetic memory devices⁸². Interesting results have been also obtained in the creation of ordered structures of semiconductor NCs doped with metallic NCs in order to tune their conductivity⁸³ and in oxide/metal binary superlattices organization for heterogeneous catalysis. In this latter case, it is worth to note that the order of the structure provides a higher thermal stability to the catalyst. Indeed, the thermally stable oxide NCs separate the metallic ones one from another, preventing their coalescence at operation temperature⁸⁴. Overall,



these results show that self-assembled superstructures are effective new materials.

However, their fabrication remains a challenge that has limited their applications. The causes of this mainly reside in the complexity and varieties of forces acting on the NCs system, and in the difficulty to control them effectively in order to guide the assembly toward the desired structure. This, however, has spurred a great effort toward the investigation of the mechanisms behind the self-assembly of colloidal NCs and a deep interest in the basic principles that make order to occurs.

1.2.1. Driving Forces for the Self-Assembly of Nanocrystals

Self-assembled structures are the result of the combined effect of all the forces acting on and among their components⁸⁵. In order to tune and project the self-assembly of NCs it is, thus, pivotal to understand which forces act on the system, how they affect the final geometry and how they can be engineered to guide the assembly toward a desired configuration. In Figure 4 are reported several successful examples of NCs self-assembly³. The structures obtained are the result of different strategies, described in the caption, aiming to control the forces present in the system. These forces could be divided in three main categories: core interactions, surface interactions and external forces, as described in details as follow:



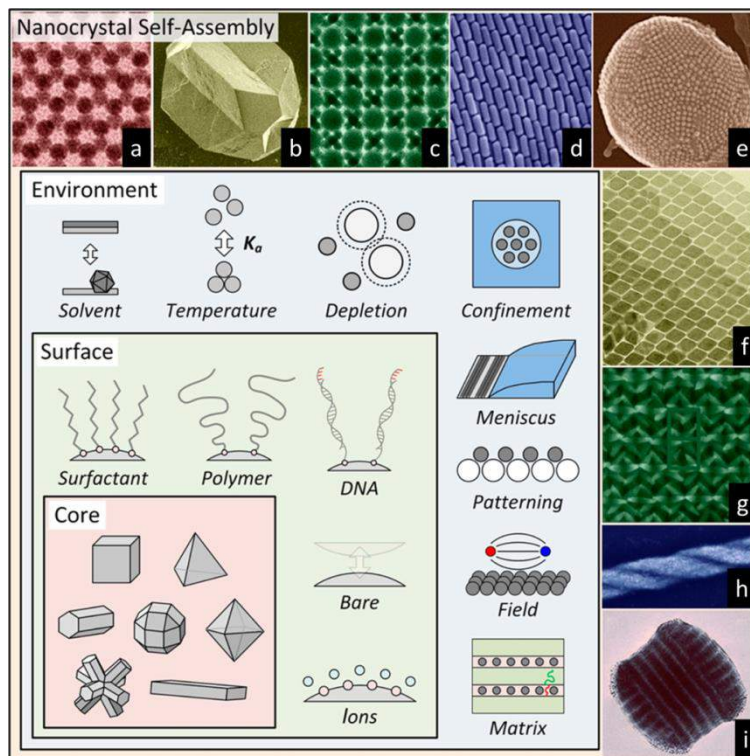


Figure 4. Scheme synthesizing how the different interactions (core, surface and external) can be combined together in order to direct the self-assembly of nanoparticles toward different structures. The figure is adapted from [3]. (a) 2D self-assembly of spherical Au NCs whose packing have been modified by proper choice of ligands (octadecanethiol)⁸⁶. (b) 3D superstructure of PbS NCs. The twinning of the facets is achieved modifying the size of the particles⁸⁷. (c) binary assembly of spherical PbS (10 nm) and Au (3 nm) NCs. The superlattice, isostructural to CaB_6 , was achieved by properly selecting the sizes of its components⁸⁸. (d) Smectic-like structure obtained employing elongated Au nanorods with 2.9 aspect ratio⁷¹. (e) cluster of spherical 9 nm CoFe_2O_4 NCs with icosahedral symmetry formed by confinement of the particles in apolar droplets formed in an oil-in-water emulsion⁸⁹. (f) columnar liquid-crystalline structure formed by rhombic GdF_3 NCs when the particles are confined at a liquid-air interface by solvent evaporation⁹⁰. (g) 3D interlocked structure created employing concave multi-branched CdSe/CdS particles¹². (h) Chiral assembly of magnetic Fe_3O_4 nanocubes formed by the anisotropic NCs at a liquid-air interface in presence of an external magnetic field⁹¹. (i) colloidal superparticle formed by CdSe/CdS rod-shaped NCs via single-particle micellae formation and successive controlled destabilization⁹².



Core Interactions

The core interactions among NCs are directly related to the properties of the solid core that forms the body of the particles: size, shape and magnetic moment.

The size and shape of the NCs dictates their “hard particle”⁹³ behaviour that results in entropic interactions, i.e. how the particles can fill the space. This interactions are usually repulsive and based on the steric hindrance that a body presents to another body moving toward it. However, in the case of attractive depletion⁹³, entropic interactions can cause an effective attraction between particles. In this situation the particles must be immersed in a mobile phase made of (or rich in) smaller objects, usually polymer chains. When two particles come close enough that no smaller object can fit among them, they experience a net osmotic pressure that pushes them together in order to eliminate the volume without smaller objects⁶.

These entropic interactions can be tuned acting on the synthesis of the NCs, modifying their size and shape. The shape of the particles, in particular, plays a fundamental role in directing the symmetry of the final structure as it dictates the configuration that particles have to keep in order to achieve the densest packing and entropy minimization⁹⁴. For this reason spherical NCs will prefer *fcc* or *hcp* packing⁹⁵, while cubic ones will form a structures with simple cubic symmetry group⁹⁴.

The presence of a net magnetic moment on NCs, finally, introduces an intrinsic directional interaction in the system. This can lead the particles to align along the crystallographic direction in which the magnetic moment lies, creating an axial order and lack of inversion symmetry in the final structure⁹⁶.



Surface Interactions

The surface interactions among NCs are usually ascribed to the interplays among the ligand shells coating the particles surfaces, which provide them with a certain degree of “soft particle” behaviour³. Given the high surface-to-volume ratio, this kind of interaction plays a considerable role in the self-assembly of NCs and, being the surface the most accessible region of the particles, this interactions are the easiest ones to tune via post-synthesis treatment such as ligand exchange. van der Waals (vdW) interactions and dipole-dipole interactions are the main players along with “soft” ligand-ligand steric repulsion.

On the surface of the particles, moreover, a net charge can be present, introducing long-range electrostatic interactions in the system. This surface charge depends from both the inorganic surface⁹⁷ and the ligand shell⁹⁸. Indeed, surface charging may arise from incomplete passivation of some facets or from ionic moieties present in the ligand shell. Moreover, electrostatic interactions are strongly influenced by the medium in which the particles are suspended, as its polarizability or the presence of dissolved ions might screen the surface charge of the NCs⁶. In addition, pH changes in the environment may force protonation or deprotonation of moieties in the ligand shell, allowing to modify the net charge at the NCs surface⁹⁹. Electrostatic interaction have been used to enhance recognition of particles with opposite charge to promote binary self-assembly¹⁰⁰ and to reduce the attraction of particles of the same kind in order to obtain less dense packing³.

Dipole interaction, which is due to permanent dipoles present in the ligand shell, is usually too weak to promote ordered assembly, as the dipoles present on the ligands are usually randomly aligned by molecular motion and do not act cooperatively⁶. However, interesting examples can be found employing two peculiar NCs coating: photo-switchable azobenzene¹⁰¹ and complementary DNA



strands¹⁰². In the first case, the ligand coating of NCs is enriched with molecules exhibiting a photo-isomerizable azobenzene group. Under UV radiation the azobenzene switches from the *trans* form (without dipole momentum) to the *cis* form (with dipole momentum) promoting nanoparticles aggregation in ordered structures. When visible light is then shone on the structure the azobenzene moieties come back to *cis* form and the particles are re-dispersed, obtaining reversible self-assembly¹⁰¹. Particles functionalization with complementary DNA strands, meanwhile, is the most precise way, at the moment, to program self-assembly¹⁰³. Thanks to (i) the strength of the hydrogen bonds (the strongest dipole-dipole interactions¹⁰⁴) that nitrogenous bases can form, (ii) to the selectivity of this bonds toward the complementary base and (iii) to the possibility to have controlled succession of bases, the structures formed by DNA-coated NCs can be programmed a-priori¹⁰³. Using self-complementary strands on the NCs surface, for example, brings toward dense packing (*fcc*, *hcp*), while using non self-complementary ones forces to introduce a second, complementary-functionalized component to achieve ordered assembly. In this case, the structure will show the less dense body centred cubic (*bcc*) symmetry¹⁰⁵. On the other hand, introducing and removing unbounded DNA strands from an assembling system allows for the tuning of the spacing between particles¹⁰⁶. Another way to exploit the DNA is to employ properly functionalized, preformed rigid DNA structures (DNA origami) as scaffold to guide the particles arrangement¹⁰⁷.

As described, electrostatic and dipolar interactions derives from peculiar precise choice of the molecules composing the ligand shell. vdW interactions, on the other hand, are ubiquitous in systems of NCs³. They are, indeed, generated by the fluctuation of local electrical potential due to electrons, so they cannot be removed... Their main effect is to drive the particles together to form aggregates, but a careful tailoring of the thickness and the density



of the ligand shell allows to prevent such aggregation or to guide it toward ordered structures⁶.

Since all these interactions take place at the surface of NCs, it is clear that the shape of the particles is extremely relevant in dictating their local intensities and their directionality. For example, having a facet which is more prone than others toward ligand functionalization, may result in patchiness in the ligand shells. This modifies the local ligand-ligand interactions, and the symmetry of the final assemblies^{108,109}. On the other way, carrying out a complete ligand exchange with DNA on strongly faceted particles allows for the realization of complex structures¹³. In this case, given the linearity of the DNA-DNA bond, the particles disposition must conform to the shape of the NCs. Finally, the density of ligands on each facet of a NC might be different due to the arrangement of the atoms exposed that serve as anchors for ligands, modifying the local strength of surface interactions¹¹⁰.

External Forces

Core and surface interactions are usually be enough to induce ordered aggregation of particles from a dispersion. However, the application of external forces to the system provides an additional tool to control the final assembly. For example, the application of an electric field to a system of polarizable NCs¹¹¹ would induce the components to assemble following the field lines. The same effect is produced by a magnetic field applied to magnetic NCs¹¹². Carrying out the assembly on a patterned substrate, meanwhile, could force the particles to follow the pattern¹¹³, as it happens when the particles are assembled in ordered matrixes like block copolymers¹¹⁴. The presence of a matrix, moreover, can modify the disposition of the particles as it can mediate or screen the particle-particle interactions¹¹⁵. Finally, the introduction of an interface where the



assembly is carried out would force the particles to deal with it, experiencing absorption toward it, reduced translational or rotational freedom, templating effect, capillary attraction,...^{116,117}

1.2.2. Strategies for the Self-Assembly of Colloidal Nanocrystals

By understanding the forces that can lead the self-assembly of NCs, have helped to develop experimental techniques to guide and control this mechanism and produce ordered structure. The common starting point is a stable dispersion of particles in Brownian motion inside a liquid medium (solvent). From this initial situation various paths can be exploited to induce the self-assembly (Figure 5)¹¹⁸.

The most straight forward tool to obtain solid aggregates consists in destabilizing the starting colloidal mixture by adding a poor dissolving liquid (antisolvent). In this way, ligand-ligand interactions becomes more favourable than ligand-solvent interactions (Figure 5a)³. Another strategy to induce particle aggregation in solution is to exploit the attractive depletion generated by the addition of voluminous molecules in solution (Figure 5b)¹¹⁹. The order of the assembly, in these situations, will be dictated by core and surface interactions, that can thus be tuned, prior to the assembly. This can be done by modifications on the NCs shape and ligand coating. Self-assembly in solution can also be induced directly acting on the ligand shell of the particles, introducing surfactants able to connect the particles, such as DNA strands¹³ or other molecular likers¹²⁰ (Figure 5c).

Another general strategy for the realization of solid structures resides in the solvent evaporation, which brings the suspension to oversaturation and thus, aggregation of NCs (Figure 5f)³. Solvent evaporation can be carried out in different ways, depending on the



evaporation rate, type of substrate, solvent and particle concentration.

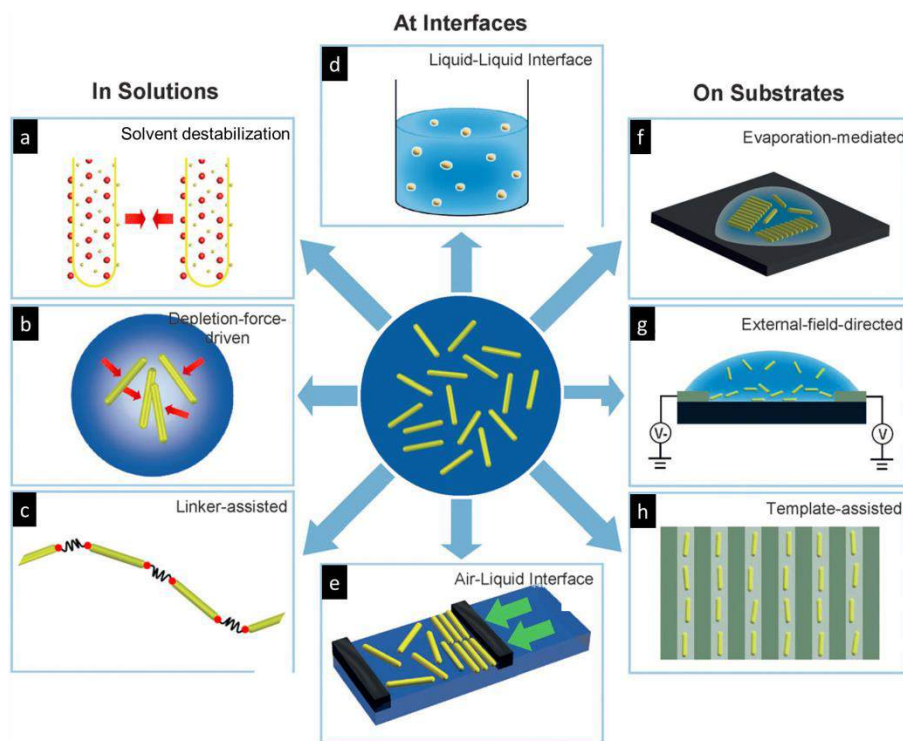


Figure 5. Examples of self-assembly techniques employed for the realization of ordered structures of nanorods from stable dispersions. The assembly may occur in solution via solvent destabilization by addition of antisolvents (**a**), via attractive depletion mediated by voluminous molecules (**b**) or with the assistance of molecular linkers (**b**). The creation of liquid-liquid interfaces (**d**) and liquid-air interfaces (**e**) is a common method to direct the assembly by constraining the movement of the particles. Finally, the assembly may take place on a solid substrate via evaporation-mediated processes (**f**) or by the guiding presence of external fields (**g**) or templates (**h**). This example can be easily extended to NCs morphologies different from rods. Figure adapted from [118].

For example, diluted dispersions of NCs can be gently drop cast on the top of a solid substrate and allowed to evaporate at open air, or under a controlled atmosphere to slow down the process. During this process, ordered assemblies can be reached either by simple



precipitation¹²¹ or by adsorption of the particles at liquid-air interface¹²². In the former case 3D ordered structures can be created, , while in the later 2D membranes (planar superlattices).

These basic tools can, then, be combined with the external forces discussed above to increment the control over the self-assembly mechanism and create new arrangement of NCs (Figure 5g,h). For example, the assembly of magnetic nanocubes at liquid-liquid interface in the presence of a magnetic field can be tailored to result in double helixes structures. Such complex structure is a compromise between the shape-dictated preferential face-to-face alignment of the cubes and the field-induced alignment along their magnetic easy axes (cube diagonal)⁹¹. Another significant example is the drop cast and annealing of a mixture of nanorods and block-copolymer¹²³. In this situation the self-assembled structure of the copolymer will serve as templating matrix for the guest NCs. These examples denotes that the careful tailoring of core and surface interactions, combined with the imposition of external forces, along with the choice of the proper self-assembly technique, can bring a complete set of experimental strategies to guide the organization of NCs from the angstrom scale up to the macroscale³.

1.3 Thesis Outline

The present thesis starts with the synthesis of a class of branched NCs with different sizes, and their structural, optical and surface characterization (Chapter 2). The assembly behaviour of such particles is, then, studied under three different conditions: (i) self-assembly of single components with different sizes and ligand shells (Chapter 3); (ii) self-assembly of binary mixtures of shape-complementary components (Chapter 4); and (iii) self-assembly in free-standing NCs-polymer composites (Chapter 5). In details, Chapter 3 describes the formation of 2D membranes made of NCs with octapod shape and shows how the arrangement of the



assembly changes from square lattices to tightly interlock chains, depending on both the size of the particles and the distribution of their ligand coating. In Chapter 4, this knowledge is employed to create 2D planar superlattices composed by two components, where octapods standing on four tips host spherical NCs. In the same chapter it is also presented an ongoing project that aims to the creation of highly complex ordered 3D structures made of two components with anisotropic shapes, octapods and cubes. In order to induce electrostatic attraction between the components, the particles have been subjected to ligand exchange with charged surfactants, tuning the ζ -potential of branched NCs from -34 mV to +7 mV. The 3D assembly of water-soluble octapods confirmed that the induced surface charge can prevent the tight interlocking of the particle, typically observed from as-synthesized one. The binary assembly, carried out with negatively charged cubes, then, showed that a proper combination of electrostatic interactions between particles with different ζ -potential and shape complementarity is able to induce local order among trios of particles. However, solubility differences among the two kinds of NCs still hinder the achievement of long-range order. In Chapter 5, the ability of octapods to form interlocked structures inside a polymer matrix is investigated by preparing NCs-polymer composite via slow solvent evaporation. The presence of such self-assembled structures was also demonstrated to improve the mechanical robustness of the resulting composite film by preventing the slippage of polymer chains. Finally, in Chapter 6, the synthesis and characterization of new fluorescent anisotropic NCs is presented, together with a preliminary investigation of their self-assembly behaviour. Using fluorescent CdSe nanoplatelets as seeds for the synthesis of CdSe/CdS octapods, a new type of anisotropic particles was synthesized. The particles are formed by an elongated body with four pods with tetrahedral symmetry at each corner. The body contains the original CdSe platelet embedded in a sphalerite CdS



shell, while the pods are formed by wurtzite CdS. The particles were found to emit at 660 nm with a maximum quantum yield of 10%. Comparing this emission to the one showed by the starting seeds (emission peak at 516 nm and 85% quantum yield), suggests the creation of a type II material. When assembled in planar membranes, these NCs were found to form nanoribbons with the main axis either parallel or perpendicular to the substrate.

Following the last chapter four main appendixes are included in the present thesis: Appendix A, in which the morphological characteristics of the NCs described in Chapter 2 are reported.

- Appendix B, that contains the results of numerical simulations of the planar self-assembly of branched NCs discussed in Chapter 3
- Appendix C, in which a detailed list of the chemicals employed for all the experimental processes are provided.
- Appendix D, that describe in details the characterization techniques employed in the various chapters.

The experimental work presented in this thesis have been performed in the facilities of the Istituto Italiano di Tecnologia in via Morego 30, 16163 Genova (GE), Italy (EU).



1.4 References

- 1 ISO/TS 80004-2:2015 Nanotechnologies - Vocabulary - Part 2: Nano-Objects.
<https://www.iso.org/obp/ui/#iso:std:iso:ts:80004:-2:ed-1:v1:en>.
- 2 Kastner, M. A. Artificial atoms. *Physics today* **46**, 24-24 (1993).
- 3 Boles, M. A., Engel, M. & Talapin, D. V. Self-Assembly of Colloidal Nanocrystals: From Intricate Structures to Functional Materials. *Chemical Reviews* **116**, 11220-11289, doi:10.1021/acs.chemrev.6b00196 (2016).
- 4 Boncheva, M. & Whitesides, G. M. Making Things by Self-Assembly. *MRS Bulletin* **30**, 736-742, doi:doi:10.1557/mrs2005.208 (2005).
- 5 Gersten, J. I. & Smith, F. W. *The Physics and Chemistry of Materials*. 826 (John Wiley & Sons, Inc., 2001).
- 6 Bishop, K. J. M., Wilmer, C. E., Soh, S. & Grzybowski, B. A. Nanoscale Forces and Their Uses in Self-Assembly. *Small* **5**, 1600-1630, doi:10.1002/smll.200900358 (2009).
- 7 Damasceno, P. F., Engel, M. & Glotzer, S. C. Predictive Self-Assembly of Polyhedra into Complex Structures. *Science* **337**, 453-457, doi:10.1126/science.1220869 (2012).
- 8 Glotzer, S. C. & Solomon, M. J. Anisotropy of building blocks and their assembly into complex structures. *Nature Materials* **6**, 557-562, doi:10.1038/nmat1949 (2007).
- 9 Manna, L., Scher, E. C. & Alivisatos, A. P. Synthesis of Soluble and Processable Rod-, Arrow-, Teardrop-, and Tetrapod-Shaped CdSe Nanocrystals. *Journal of the American Chemical Society* **122**, 12700-12706, doi:10.1021/ja003055+ (2000).



- 10 Paik, T. & Murray, C. B. Shape-Directed Binary Assembly of Anisotropic Nanoplates: A Nanocrystal Puzzle with Shape-Complementary Building Blocks. *Nano Letters* **13**, 2952-2956, doi:10.1021/nl401370n (2013).
- 11 Deka, S. *et al.* Octapod-Shaped Colloidal Nanocrystals of Cadmium Chalcogenides via “One-Pot” Cation Exchange and Seeded Growth. *Nano Letters* **10**, 3770-3776, doi:10.1021/nl102539a (2010).
- 12 Miszta, K. *et al.* Hierarchical self-assembly of suspended branched colloidal nanocrystals into superlattice structures. *Nature Materials* **10**, 872-876, doi:10.1038/nmat3121 (2011).
- 13 O'Brien, M. N., Jones, M. R., Lee, B. & Mirkin, C. A. Anisotropic nanoparticle complementarity in DNA-mediated co-crystallization. *Nature Materials* **14**, 833-839, doi:10.1038/nmat4293 (2015).
- 14 Murray, C. B. *et al.* Colloidal synthesis of nanocrystals and nanocrystal superlattices. *IBM Journal of Research and Development* **45**, 47-56 (2001).
- 15 Zherebetsky, D. *et al.* Hydroxylation of the surface of PbS nanocrystals passivated with oleic acid. *Science* **344**, 1380-1384, doi:10.1126/science.1252727 (2014).
- 16 Murray, C., Norris, D. J. & Bawendi, M. G. Synthesis and characterization of nearly monodisperse CdE (E= sulfur, selenium, tellurium) semiconductor nanocrystallites. *Journal of the American Chemical Society* **115**, 8706-8715 (1993).
- 17 Rao, J. P. & Geckeler, K. E. Polymer nanoparticles: preparation techniques and size-control parameters. *Progress in Polymer Science* **36**, 887-913 (2011).
- 18 Vichery, C. & Nedelec, J.-M. Bioactive glass nanoparticles: from synthesis to materials design for biomedical applications. *Materials* **9**, 288 (2016).
- 19 Quarta, A., Curcio, A., Kakwere, H. & Pellegrino, T. Polymer coated inorganic nanoparticles: tailoring the



- nanocrystal surface for designing nanoprobes with biological implications. *Nanoscale* **4**, 3319-3334 (2012).
- 20 Kovalenko, M. V., Scheele, M. & Talapin, D. V. Colloidal nanocrystals with molecular metal chalcogenide surface ligands. *Science* **324**, 1417-1420 (2009).
- 21 Thanh, N. T. K., Maclean, N. & Mahiddine, S. Mechanisms of Nucleation and Growth of Nanoparticles in Solution. *Chemical Reviews* **114**, 7610-7630, doi:10.1021/cr400544s (2014).
- 22 Murray, C. B., Kagan, C. R. & Bawendi, M. G. Synthesis and Characterization of Monodisperse Nanocrystals and Close-Packed Nanocrystal Assemblies. *Annual Review of Materials Science* **30**, 545-610, doi:10.1146/annurev.matsci.30.1.545 (2000).
- 23 LaMer, V. K. & Dinegar, R. H. Theory, production and mechanism of formation of monodispersed hydrosols. *Journal of the American Chemical Society* **72**, 4847-4854 (1950).
- 24 Yin, Y. & Alivisatos, A. P. Colloidal nanocrystal synthesis and the organic-inorganic interface. *Nature* **437**, 664-670 (2005).
- 25 Brazeau, A. L. & Jones, N. D. Growth Mechanisms in Nanocrystalline Lead Sulfide by Stopped-Flow Kinetic Analysis. *The Journal of Physical Chemistry C* **113**, 20246-20251 (2009).
- 26 Woehl, T. J., Evans, J. E., Arslan, I., Ristenpart, W. D. & Browning, N. D. Direct in situ determination of the mechanisms controlling nanoparticle nucleation and growth. *ACS Nano* **6**, 8599-8610, doi:10.1021/nn303371y (2012).
- 27 Bastús, N. G., Comenge, J. & Puntès, V. Kinetically Controlled Seeded Growth Synthesis of Citrate-Stabilized Gold Nanoparticles of up to 200 nm: Size Focusing versus Ostwald Ripening. *Langmuir* **27**, 11098-11105, doi:10.1021/la201938u (2011).



- 28 Liu, X., Atwater, M., Wang, J. & Huo, Q. Extinction coefficient of gold nanoparticles with different sizes and different capping ligands. *Colloids and Surfaces B: Biointerfaces* **58**, 3-7 (2007).
- 29 Roduner, E. Size matters: why nanomaterials are different. *Chemical Society Reviews* **35**, 583-592, doi:10.1039/B502142C (2006).
- 30 Kohn, A., Weigend, F. & Ahlrichs, R. Theoretical study on clusters of magnesium. *Physical Chemistry Chemical Physics* **3**, 711-719, doi:10.1039/B007869G (2001).
- 31 Hou, M. Solid-liquid and liquid-solid transitions in metal nanoparticles. *Physical Chemistry Chemical Physics* **19**, 5994-6005, doi:10.1039/C6CP08606C (2017).
- 32 Schmidt, M. *et al.* Negative Heat Capacity for a Cluster of 147 Sodium Atoms. *Physical Review Letters* **86**, 1191-1194 (2001).
- 33 Norris, D. J. & Bawendi, M. G. Measurement and assignment of the size-dependent optical spectrum in CdSe quantum dots. *Physical Review B* **53**, 16338-16346 (1996).
- 34 Alivisatos, A. Semiconductor clusters, nanocrystals, and quantum dots. *Science* **271**, 933 (1996).
- 35 Ashoori, R. C. Electrons in artificial atoms. *Nature* **379**, 413-419 (1996).
- 36 Yanhong, L., Dejun, W., Qidong, Z., Min, Y. & Qinglin, Z. A Study of Quantum Confinement Properties of Photogenerated Charges in ZnO Nanoparticles by Surface Photovoltage Spectroscopy. *The Journal of Physical Chemistry B* **108**, 3202-3206, doi:10.1021/jp037201k (2004).
- 37 Mock, J., Barbic, M., Smith, D., Schultz, D. & Schultz, S. Shape effects in plasmon resonance of individual colloidal silver nanoparticles. *The Journal of Chemical Physics* **116**, 6755-6759 (2002).



- 38 Burda, C., Chen, X., Narayanan, R. & El-Sayed, M. A. Chemistry and properties of nanocrystals of different shapes. *Chemical reviews* **105**, 1025-1102 (2005).
- 39 Bera, D., Qian, L., Tseng, T.-K. & Holloway, P. H. Quantum dots and their multimodal applications: a review. *Materials* **3**, 2260-2345 (2010).
- 40 Klein, D. L., Roth, R., Lim, A. K. L., Alivisatos, A. P. & McEuen, P. L. A single-electron transistor made from a cadmium selenide nanocrystal. *Nature* **389**, 699, doi:10.1038/39535 (1997).
- 41 Anikeeva, P. O., Halpert, J. E., Bawendi, M. G. & Bulovic, V. Quantum dot light-emitting devices with electroluminescence tunable over the entire visible spectrum. *Nano letters* **9**, 2532-2536 (2009).
- 42 Mashford, B. S. *et al.* High-efficiency quantum-dot light-emitting devices with enhanced charge injection. *Nature Photonics* **7**, 407-412, doi:10.1038/nphoton.2013.70 (2013).
- 43 Shirasaki, Y., Supran, G. J., Bawendi, M. G. & Bulović, V. Emergence of colloidal quantum-dot light-emitting technologies. *Nature Photonics* **7**, 13-23, doi:10.1038/nphoton.2012.328 (2012).
- 44 Eisler, H.-J. *et al.* Color-selective semiconductor nanocrystal laser. *Applied Physics Letters* **80**, 4614-4616, doi:10.1063/1.1485125 (2002).
- 45 Klimov, V. I. *et al.* Optical Gain and Stimulated Emission in Nanocrystal Quantum Dots. *Science* **290**, 314-317, doi:10.1126/science.290.5490.314 (2000).
- 46 Pisanello, F. *et al.* Dots in rods as polarized single photon sources. *Superlattices and Microstructures* **47**, 165-169 (2010).
- 47 Ithurria, S. *et al.* Colloidal nanoplatelets with two-dimensional electronic structure. *Nature Materials* **10**, 936-941, doi:10.1038/nmat3145 (2011).



- 48 Becker, J., Trügler, A., Jakab, A., Hohenester, U. & Sönnichsen, C. The optimal aspect ratio of gold nanorods for plasmonic bio-sensing. *Plasmonics* **5**, 161-167 (2010).
- 49 Tan, S. J., Campolongo, M. J., Luo, D. & Cheng, W. Building plasmonic nanostructures with DNA. *Nature Nanotechnology* **6**, 268-276, doi:10.1038/nnano.2011.49 (2011).
- 50 Barmparis, G. D., Lodziana, Z., Lopez, N. & Remediakis, I. N. Nanoparticle shapes by using Wulff constructions and first-principles calculations. *Beilstein Journal of Nanotechnology* **6**, 361-368, doi:10.3762/bjnano.6.35 (2015).
- 51 Tao, A., Sinsermuksakul, P. & Yang, P. Polyhedral silver nanocrystals with distinct scattering signatures. *Angewandte Chemie* **118**, 4713-4717 (2006).
- 52 Huang, M. H. & Lin, P. H. Shape-Controlled Synthesis of Polyhedral Nanocrystals and Their Facet-Dependent Properties. *Advanced Functional Materials* **22**, 14-24 (2012).
- 53 Vitos, L., Ruban, A., Skriver, H. L. & Kollar, J. The surface energy of metals. *Surface Science* **411**, 186-202 (1998).
- 54 Sau, T. K. & Murphy, C. J. Room temperature, high-yield synthesis of multiple shapes of gold nanoparticles in aqueous solution. *Journal of the American Chemical Society* **126**, 8648-8649 (2004).
- 55 Habas, S. E., Lee, H., Radmilovic, V., Somorjai, G. A. & Yang, P. Shaping binary metal nanocrystals through epitaxial seeded growth. *Nature Materials* **6**, 692-697 (2007).
- 56 Hamadianian, M., Reisi-Vanani, A. & Majedi, A. Synthesis, characterization and effect of calcination temperature on phase transformation and photocatalytic activity of Cu, S-codoped TiO₂ nanoparticles. *Applied Surface Science* **256**, 1837-1844 (2010).



- 57 De Trizio, L. & Manna, L. Forging Colloidal Nanostructures via Cation Exchange Reactions. *Chemical Reviews* **116**, 10852-10887, doi:10.1021/acs.chemrev.5b00739 (2016).
- 58 Hodges, J. M., Kletetschka, K., Fenton, J. L., Read, C. G. & Schaak, R. E. Sequential Anion and Cation Exchange Reactions for Complete Material Transformations of Nanoparticles with Morphological Retention. *Angewandte Chemie International Edition* **54**, 8669-8672, doi:10.1002/anie.201504099 (2015).
- 59 Carbone, L. *et al.* Synthesis and Micrometer-Scale Assembly of Colloidal CdSe/CdS Nanorods Prepared by a Seeded Growth Approach. *Nano Letters* **7**, 2942-2950, doi:10.1021/nl0717661 (2007).
- 60 Najafshirvari, S. *et al.* The effect of Au domain size on the CO oxidation catalytic activity of colloidal Au-FeO_x dumbbell-like heterodimers. *Journal of Catalysis* **338**, 115-123 (2016).
- 61 Fan, H. J., Gösele, U. & Zacharias, M. Formation of nanotubes and hollow nanoparticles based on Kirkendall and diffusion processes: a review. *Small* **3**, 1660-1671, doi:10.1002/smll.200700382 (2007).
- 62 Milliron, D. J. *et al.* Colloidal nanocrystal heterostructures with linear and branched topology. *Nature* **430**, 190-195 (2004).
- 63 Boisselier, E. & Astruc, D. Gold nanoparticles in nanomedicine: preparations, imaging, diagnostics, therapies and toxicity. *Chemical Society Reviews* **38**, 1759-1782, doi:10.1039/B806051G (2009).
- 64 Guardia, P. *et al.* Water-Soluble Iron Oxide Nanocubes with High Values of Specific Absorption Rate for Cancer Cell Hyperthermia Treatment. *ACS Nano* **6**, 3080-3091, doi:10.1021/nn2048137 (2012).



- 65 Talapin, D. V., Lee, J.-S., Kovalenko, M. V. & Shevchenko, E. V. Prospects of Colloidal Nanocrystals for Electronic and Optoelectronic Applications. *Chemical Reviews* **110**, 389-458, doi:10.1021/cr900137k (2010).
- 66 Protesescu, L. *et al.* Nanocrystals of Cesium Lead Halide Perovskites (CsPbX₃, X = Cl, Br, and I): Novel Optoelectronic Materials Showing Bright Emission with Wide Color Gamut. *Nano Letters* **15**, 3692-3696, doi:10.1021/nl5048779 (2015).
- 67 Gilroy, K. D., Ruditskiy, A., Peng, H.-C., Qin, D. & Xia, Y. Bimetallic Nanocrystals: Syntheses, Properties, and Applications. *Chemical Reviews* **116**, 10414-10472, doi:10.1021/acs.chemrev.6b00211 (2016).
- 68 Zhou, Z.-Y., Tian, N., Li, J.-T., Broadwell, I. & Sun, S.-G. Nanomaterials of high surface energy with exceptional properties in catalysis and energy storage. *Chemical Society Reviews* **40**, 4167-4185, doi:10.1039/C0CS00176G (2011).
- 69 Wu, Z.-S. *et al.* Graphene Anchored with Co₃O₄ Nanoparticles as Anode of Lithium Ion Batteries with Enhanced Reversible Capacity and Cyclic Performance. *ACS Nano* **4**, 3187-3194, doi:10.1021/nn100740x (2010).
- 70 Augustyn, V. *et al.* High-rate electrochemical energy storage through Li⁺ intercalation pseudocapacitance. *Nature Materials* **12**, 518, doi:10.1038/nmat3601 (2013).
- 71 Ye, X. *et al.* Improved size-tunable synthesis of monodisperse gold nanorods through the use of aromatic additives. *ACS nano* **6**, 2804-2817 (2012).
- 72 Li, L.-s., Walda, J., Manna, L. & Alivisatos, A. P. Semiconductor nanorod liquid crystals. *Nano Letters* **2**, 557-560 (2002).
- 73 Shevchenko, E. V., Talapin, D. V., Kotov, N. A., O'Brien, S. & Murray, C. B. Structural diversity in binary nanoparticle



- superlattices. *Nature* **439**, 55-59, doi:10.1038/nature04414 (2006).
- 74 Boneschanscher, M. P. *et al.* Long-range orientation and atomic attachment of nanocrystals in 2D honeycomb superlattices. *Science* **344**, 1377-1380, doi:10.1126/science.1252642 (2014).
- 75 Kagan, C. R., Murray, C. B., Nirmal, M. & Bawendi, M. G. Electronic Energy Transfer in CdSe Quantum Dot Solids. *Physical Review Letters* **76**, 1517-1520 (1996).
- 76 Rizzo, A. *et al.* Polarized Light Emitting Diode by Long-Range Nanorod Self-Assembling on a Water Surface. *ACS Nano* **3**, 1506-1512, doi:10.1021/nm900063m (2009).
- 77 Lu, F. *et al.* Discrete Nanocubes as Plasmonic Reporters of Molecular Chirality. *Nano Letters* **13**, 3145-3151, doi:10.1021/nl401107g (2013).
- 78 Ye, X., Chen, J., Diroll, B. T. & Murray, C. B. Tunable plasmonic coupling in self-assembled binary nanocrystal superlattices studied by correlated optical microspectrophotometry and electron microscopy. *Nano Letters* **13**, 1291-1297, doi:10.1021/nl400052w (2013).
- 79 Nie, S. & Emory, S. R. Probing Single Molecules and Single Nanoparticles by Surface-Enhanced Raman Scattering. *Science* **275**, 1102-1106 (1997).
- 80 Lin, Q.-Y. *et al.* Strong coupling between plasmonic gap modes and photonic lattice modes in DNA-assembled gold nanocube arrays. *Nano Letters* **15**, 4699-4703 (2015).
- 81 Shevchenko, E. V. *et al.* Self-Assembled Binary Superlattices of CdSe and Au Nanocrystals and Their Fluorescence Properties. *Journal of the American Chemical Society* **130**, 3274-3275, doi:10.1021/ja710619s (2008).
- 82 Chen, J. *et al.* Collective Dipolar Interactions in Self-Assembled Magnetic Binary Nanocrystal Superlattice



- Membranes. *Nano Letters* **10**, 5103-5108, doi:10.1021/nl103568q (2010).
- 83 Urban, J. J., Talapin, D. V., Shevchenko, E. V., Kagan, C. R. & Murray, C. B. Synergism in binary nanocrystal superlattices leads to enhanced p-type conductivity in self-assembled PbTe/Ag₂Te thin films. *Nature Materials* **6**, 115-121, doi:10.1038/nmat1826 (2007).
- 84 Kang, Y. *et al.* Engineering catalytic contacts and thermal stability: gold/iron oxide binary nanocrystal superlattices for CO oxidation. *Journal of the American Chemical Society* **135**, 1499-1505 (2013).
- 85 Whitesides, G. M. & Grzybowski, B. Self-Assembly at All Scales. *Science* **295**, 2418-2421, doi:10.1126/science.1070821 (2002).
- 86 Boles, M. A. & Talapin, D. V. Many-Body Effects in Nanocrystal Superlattices: Departure from Sphere Packing Explains Stability of Binary Phases. *Journal of the American Chemical Society* **137**, 4494-4502, doi:10.1021/jacs.5b00839 (2015).
- 87 Rupich, S. M., Shevchenko, E. V., Bodnarchuk, M. I., Lee, B. & Talapin, D. V. Size-Dependent Multiple Twinning in Nanocrystal Superlattices. *Journal of the American Chemical Society* **132**, 289-296, doi:10.1021/ja9074425 (2010).
- 88 Boles, M. A. *Self-assembly of colloidal nanocrystals: Surface ligands promote the formation of unexpected superlattices* PhD thesis, The University of Chicago, (2016).
- 89 De Nijs, B. *et al.* Entropy-driven formation of large icosahedral colloidal clusters by spherical confinement. *Nature Materials* **14**, 56-60, doi:10.1038/nmat4072 (2015).
- 90 Paik, T., Ko, D.-K., Gordon, T. R., Doan-Nguyen, V. & Murray, C. B. Studies of Liquid Crystalline Self-Assembly of GdF₃ Nanoplates by In-Plane, Out-of-Plane SAXS. *ACS Nano* **5**, 8322-8330, doi:10.1021/nn203049t (2011).



- 91 Singh, G. *et al.* Self-assembly of magnetite nanocubes into helical superstructures. *Science* **345**, 1149-1153, doi:10.1126/science.1254132 (2014).
- 92 Wang, T. *et al.* Self-Assembled Colloidal Superparticles from Nanorods. *Science* **338**, 358-363, doi:10.1126/science.1224221 (2012).
- 93 Asakura, S. & Oosawa, F. On interaction between two bodies immersed in a solution of macromolecules. *The Journal of Chemical Physics* **22**, 1255-1256 (1954).
- 94 Quan, Z. & Fang, J. Superlattices with non-spherical building blocks. *Nano Today* **5**, 390-411, doi:<http://dx.doi.org/10.1016/j.nantod.2010.08.011> (2010).
- 95 Redl, F. X., Cho, K.-S., Murray, C. B. & O'Brien, S. Three-dimensional binary superlattices of magnetic nanocrystals and semiconductor quantum dots. *Nature* **423**, 968-971 (2003).
- 96 Tanase, M. *et al.* Magnetic alignment of fluorescent nanowires. *Nano Letters* **1**, 155-158 (2001).
- 97 Krauss, T. D. & Brus, L. E. Charge, polarizability, and photoionization of single semiconductor nanocrystals. *Physical Review Letters* **83**, 4840 (1999).
- 98 Boles, M. A., Ling, D., Hyeon, T. & Talapin, D. V. The surface science of nanocrystals. *Nature Materials* **15**, 141-153 (2016).
- 99 Du, J.-Z., Du, X.-J., Mao, C.-Q. & Wang, J. Tailor-made dual pH-sensitive polymer–doxorubicin nanoparticles for efficient anticancer drug delivery. *Journal of the American Chemical Society* **133**, 17560-17563 (2011).
- 100 Kalsin, A. M. *et al.* Electrostatic Self-Assembly of Binary Nanoparticle Crystals with a Diamond-Like Lattice. *Science* **312**, 420-424, doi:10.1126/science.1125124 (2006).
- 101 Klajn, R., Bishop, K. J. M. & Grzybowski, B. A. Light-controlled self-assembly of reversible and irreversible



- nanoparticle suprastructures. *Proceedings of the National Academy of Sciences* **104**, 10305-10309, doi:10.1073/pnas.0611371104 (2007).
- 102 Rogers, W. B., Shih, W. M. & Manoharan, V. N. Using DNA to program the self-assembly of colloidal nanoparticles and microparticles. *Nature Reviews Materials* **1**, 16008 (2016).
- 103 Jones, M. R., Seeman, N. C. & Mirkin, C. A. Programmable materials and the nature of the DNA bond. *Science* **347**, doi:10.1126/science.1260901 (2015).
- 104 Steiner, T. The hydrogen bond in the solid state. *Angewandte Chemie International Edition* **41**, 48-76 (2002).
- 105 Park, S. Y. *et al.* DNA-programmable nanoparticle crystallization. *Nature* **451**, 553-556 (2008).
- 106 Maye, M. M., Kumara, M. T., Nykypanchuk, D., Sherman, W. B. & Gang, O. Switching binary states of nanoparticle superlattices and dimer clusters by DNA strands. *Nature Nanotechnology* **5**, 116-120 (2010).
- 107 Liu, W. *et al.* Diamond family of nanoparticle superlattices. *Science* **351**, 582-586 (2016).
- 108 Choi, J. J. *et al.* Controlling nanocrystal superlattice symmetry and shape-anisotropic interactions through variable ligand surface coverage. *Journal of the American Chemical Society* **133**, 3131-3138 (2011).
- 109 Nie, Z. *et al.* Self-assembly of metal-polymer analogues of amphiphilic triblock copolymers. *Nature Materials* **6**, 609-614 (2007).
- 110 Ye, X. *et al.* Competition of shape and interaction patchiness for self-assembling nanoplates. *Nature Chemistry* **5**, 466-473, doi:10.1038/nchem.1651 (2013).
- 111 Ryan, K. M., Mastroianni, A., Stancil, K. A., Liu, H. & Alivisatos, A. Electric-field-assisted assembly of



- perpendicularly oriented nanorod superlattices. *Nano Letters* **6**, 1479-1482 (2006).
- 112 Lalatonne, Y., Richardi, J. & Pileni, M. Van der Waals versus dipolar forces controlling mesoscopic organizations of magnetic nanocrystals. *Nature Materials* **3**, 121-125 (2004).
- 113 Cui, Y. *et al.* Integration of colloidal nanocrystals into lithographically patterned devices. *Nano Letters* **4**, 1093-1098 (2004).
- 114 Balazs, A. C., Emrick, T. & Russell, T. P. Nanoparticle Polymer Composites: Where Two Small Worlds Meet. *Science* **314**, 1107-1110, doi:10.1126/science.1130557 (2006).
- 115 Arciniegas, M. P. *et al.* Self-Assembly of Octapod-Shaped Colloidal Nanocrystals into a Hexagonal Ballerina Network Embedded in a Thin Polymer Film. *Nano Letters* **14**, 1056-1063, doi:10.1021/nl404732m (2014).
- 116 Böker, A., He, J., Emrick, T. & Russell, T. P. Self-assembly of nanoparticles at interfaces. *Soft Matter* **3**, 1231-1248 (2007).
- 117 Taniguchi, Y., Takishita, T., Kawai, T. & Nakashima, T. End-to-End Self-Assembly of Semiconductor Nanorods in Water by Using an Amphiphilic Surface Design. *Angewandte Chemie International Edition* **55**, 2083-2086, doi:10.1002/anie.201509833 (2016).
- 118 Zhang, S.-Y., Regulacio, M. D. & Han, M.-Y. Self-assembly of colloidal one-dimensional nanocrystals. *Chemical Society Reviews* **43**, 2301-2323, doi:10.1039/C3CS60397K (2014).
- 119 Zanella, M. *et al.* Assembly of shape-controlled nanocrystals by depletion attraction. *Chemical Communications* **47**, 203-205, doi:10.1039/C0CC02477E (2011).
- 120 Shibu Joseph, S. T., Ipe, B. I., Pramod, P. & Thomas, K. G. Gold Nanorods to Nanochains: Mechanistic Investigations on Their Longitudinal Assembly Using α, ω -Alkanedithiols



- and Interplasmon Coupling. *The Journal of Physical Chemistry B* **110**, 150-157, doi:10.1021/jp0544179 (2006).
- 121 Bigioni, T. P. *et al.* Kinetically driven self assembly of highly ordered nanoparticle monolayers. *Nature Materials* **5**, 265-270 (2006).
- 122 Martin, M. N., Basham, J. I., Chando, P. & Eah, S.-K. Charged Gold Nanoparticles in Non-Polar Solvents: 10-min Synthesis and 2D Self-Assembly. *Langmuir* **26**, 7410-7417, doi:10.1021/la100591h (2010).
- 123 Thorkelsson, K., Nelson, J. H., Alivisatos, A. P. & Xu, T. End-to-end alignment of nanorods in thin films. *Nano Letters* **13**, 4908-4913, doi:10.1021/nl402862b (2013).



2 Size Tuning and Surface Analysis of Branched Colloidal Nanocrystals

Octapod-shaped NCs are, along with tetrapods¹⁻³, the most studied branched particles in the self-assembly field⁴⁻⁹. Their complex shape consists of eight pods, disposed along the diagonals of an hypothetical cube, that grow from the facets of a common core with an octahedral symmetry, placed at the centre of such cube (Figure 1). Structures of this type have been realized with several materials, such as CdS¹⁰, CdSe¹¹, PbS¹², PbSe¹³, Pt^{14,15} and FePt¹⁶. However, the control gained on the shape of CdSe/CdS octapods through reproducible synthesis makes them an exemplary type of branched NCs¹⁷. Specifically, in the present thesis we use octapod NCs formed by eight wurtzite CdS pods and a sphalerite CdSe core (Figure 1). The CdS pods of such particles can be divided in two regions with different faceting: the shafts and the tips (Figure 1b). The shafts have a triangular section, grow along their $\langle 0\ 0\ 0\ 1 \rangle$ direction, expose three $\{1\ 0\ 1\ 0\}$ facets and depart from the $\{1\ 1\ 1\}$ facets of the CdSe core¹⁸. The tips, instead, are divided in two



families, four of which are flat, terminating with a $(0\ 0\ 0\ 1)$ facet, and the other four are tapered, formed by three $\{1\ 0\ 1\ \bar{1}\}$ facets (Figure 1b). The tapered tips are always opposite to the flat one, as if the particle would have been made by two tetrapods, one with flat tips and one with tapered tips, fused together at the core.

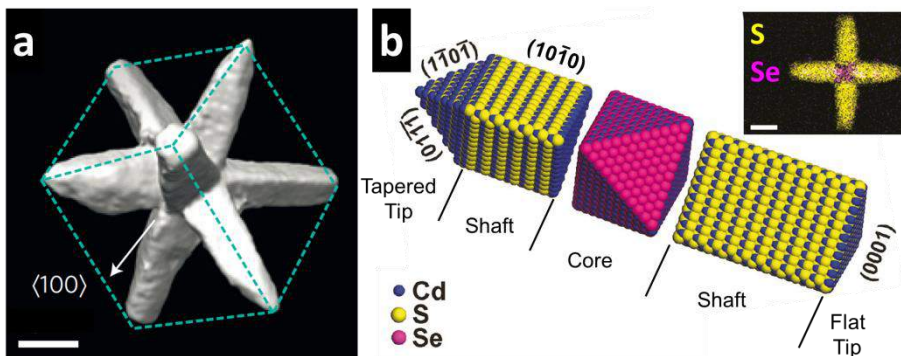


Figure 1. (a) Volume reconstruction of a CdSe/CdS core/shell octapod-shaped NCs. Scale bar: 20 nm. The dashed lines evidence the circumscribed cube. (b) Exploded sketch of an octapod NC that highlights the CdSe core and the faceting of the CdS shafts and tips. The inset shows an Energy-dispersive X-ray spectroscopy (EDS) elemental mapping of an octapod for S and Se. Scale bar: 10 nm. Images adapted from [4] (a) and [18] (b).

Thanks to this complex structure, octapods are an appealing model for studying the self-assembly of strongly anisotropic NCs. Their branched morphology, spanning over the three spatial dimensions, does not allow to identify any axes or plane of easy stacking, as it occurs in the case of nanorods (all parallel axes), or platelets (all parallel flat faces)¹⁹⁻²³. They are, thus, not limited to a preferential type of assembled architecture, but can form several different geometries that depend on the experimental conditions (Figure 2).

For instance, hierarchically 3D ordered structures are obtained by the induced aggregation of chains made by tightly interlocked octapods via solvent destabilization (Figure 2a). In another type of octapod assembly, when a drop of the suspension is evaporated on a



solid substrate, 2D arrangement of the particles is observed⁵ (Figure 2b). Depending on their pod length, octapods can form different bi-dimensional lattices⁶. Also, if the same drop cast procedure is performed from a polymer-rich solution of octapods, the particles assume a different configuration, which resembles a ballet of ballerinas (Figure 2c)⁷.

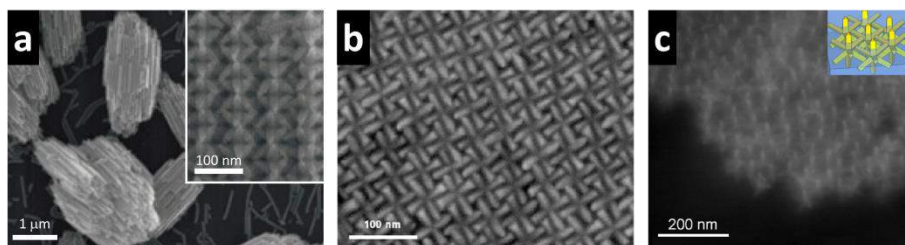


Figure 2. High resolution scanning electron microscopy (HRSEM) images of the different assembled configurations observed from CdSe/CdS octapod NCs. (a) 3D superstructures made by packing of interlocked linear arrays (inset), obtained by solution destabilization⁴; (b) Square lattice structure produced by drop cast the suspension on a flat substrate⁵; (c) Ballerina's ballet formed by octapods assembled in a polymer matrix; the brighter spots are the pods protruding outside the polymer layer⁷.

In this latter organization, the octapods touch the substrate with only one tip, while the opposite one protrudes outside the polymer thin layer (brighter spots in Figure 2c). The other six pods interact with the ones from neighbouring octapods in order to have maximum contact (parallel pod-pod configuration), giving a hexagonal symmetry to the assembled structure. The versatility toward self-assembly shown by octapods has motivated this investigation to better understand which parameters can be tuned to regulate and direct the spontaneous organization of this less explored class of NCs.

Despite the significant efforts made so far, both experimental and theoretical^{4,6,8,9}, there are many unsolved questions regarding the nature of interactions between octapods that lead to their exotic



assemblies. For example, in the case of linear arrays, numerical simulations show that, in order to aggregate them into interlocked structures, octapods must experience an attractive particle interaction of unknown origin, since shape-dictated entropic arguments do not explain this configuration^{4,24}. In addition to this, their complex synthesis has not allowed the controlled fabrication of particles with different sizes without sensibly modifying their ligand shell²⁵. It has, thus, been difficult to assess the role of the particle size in their assemblies, as well as the impact of the ligands coating their surfaces.

This chapter summarizes our efforts on overcome these issues starting from a simple optimization of the protocol employed for the synthesis of octapods, to a complete characterization of the particles. As detailed in Section 2.1, controlled modifications in the amount of CdSe seeds injected in the synthesis, allows to finely tune the size of the octapods, without changing the surfactants type and quantity. This enabled the realization of NCs with pods spanning from 13 nm up to 40 nm. Structural and morphological characterization demonstrates that differences in the pod length did not affect the intrinsic structure of the octapods, as all the particles expose the same CdS facets. The availability of particles with controllable sizes made possible to further investigate, by an extensive characterization of their surfaces, how the octapod aspect ratio affects the distribution of their ligands as detailed in Section 2.2. The assessment of an anisotropic ligand distribution on the octapod shafts described in this Chapter, is of relevance to better understand the self-assembly behaviour of octapods, as it will be discussed in Chapter 3.

The present Chapter is based on our work recently submitted article to Nature Communications [24].



2.1 Synthesis and Characterization of Branched Colloidal Nanocrystals with different sizes

The synthesis of octapods is based on a seeded growth process^{17,25}, where preformed NCs, named seeds, are employed as nucleation points for a second reaction to occur. Since the first protocol reported in 2010, the octapod synthesis involves the preparation of Cu_{2-x}Se seeds to be injected at high temperature, under the presence of four main phosphorous ligands. In the present work, we used cuboctahedra seeds that have a cubic berzelianite lattice (Figure 3).

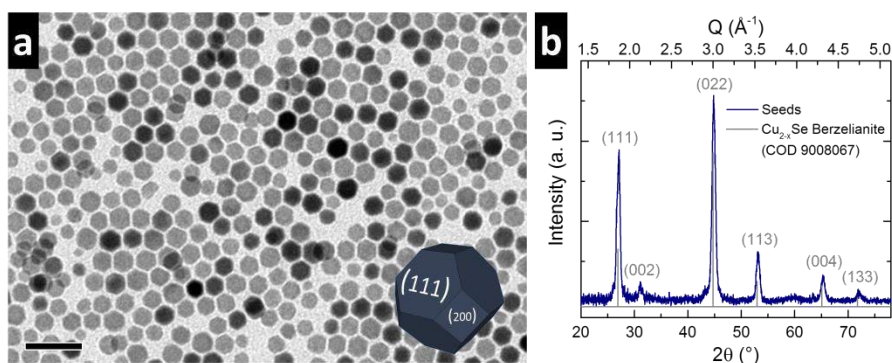


Figure 3. (a) TEM image of the Cu_{2-x}Se seeds employed in the syntheses of octapods. Their morphology is highlighted in the embedded sketch, that indicates also the two main families of crystallographic planes that form the surface of the NCs. The pods nucleation and growth in the synthesis of octapods will take place on the eight facets $\{1\ 1\ 1\}$. Scale bar: 50 nm. (b) XRD pattern collected from the synthesized Cu_{2-x}Se seeds and compared to the berzelianite structure (vertical lines).

Thanks to their faceting, these NCs act as templating agents and dictate the growth direction of the pods²⁶. To synthesize the Cu_{2-x}Se , we implemented a synthesis protocol developed by Saldanha et. al²⁷ with some modifications. In detail, in a three-neck flask 1 mmol of copper (II) acetylacetonate ($\text{Cu}(\text{acac})_2$ 262 mg) was dissolved in 9.5 ml of oleylamine (OLAM) and 3 ml of 1-dodecanetihol (DDT) and degassed for one hour at 60°C under stirring. Then, the temperature was increased to 220°C under nitrogen flow. Once the



solution became orange-brown (an indication of the formation of reactive Cu species), 1 ml of a previously prepared solution of Se (1 M in OLAM-DDT mixture 50-50 % vol.) and 1.5 ml of degassed DDT were injected in the flask. After 4 min, the solution was cooled down to room temperature. Finally, the colloidal suspension was collected in a vial and purified to eliminate the excess of ligands, by conducting three washing cycles via precipitation with methanol, centrifugation, and re-dispersion in toluene. The NCs obtained were characterized by X-ray diffraction (XRD) and transmission electron microscopy (TEM) imaging. The analysis confirmed the berzelianite structure in particles with a diameter of 14 ± 2 nm (Figure 3), as evaluated by direct TEM image analysis using ImageJ software.

In order to facilitate the discussion and before illustrating the synthesis of octapods, a brief description of the particle geometrical aspects is provided as follow. We have established four parameters to describe the octapods, as shown in the sketch in Figure 4a. They are the pod length, l_p , the tip-to-tip length, L , the pod thickness, D , and the core diameter, d_{core} .

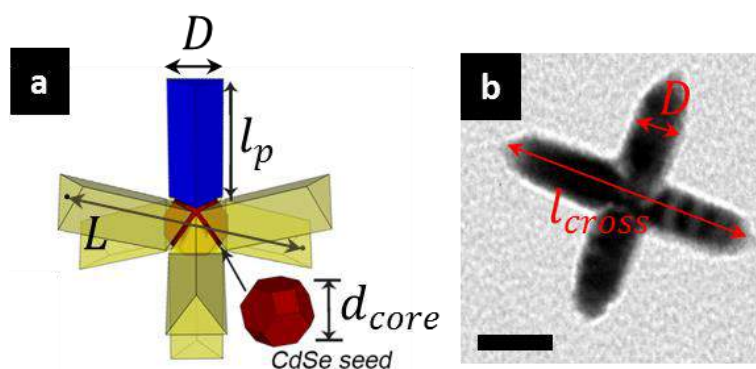


Figure 4. (a) Sketch of an octapod showing their geometrical aspects, as described in the main text. (b) TEM image of a single octapod with a cross-like projection (top view), that is, it touches the substrate with four pods. In the image, the parameters l_{cross} and D , are also shown. Scale bar: 20 nm.



The evaluation of these dimensions, for all the synthesized octapods, were conducted through careful analysis of the collected TEM images. Particles giving a cross-like projection in the images (Figure 4b) were selected to directly measure D . The L and l_p parameters were calculated by measuring first the distance between two opposite tips in the particle cross projection (l_{cross} in Figure 4b) as an equivalent of the face diagonal of the hypothetical cube surrounding the octapod. Thus, L and l_p were obtained by following equation (1) and (2).

$$L = \sqrt{\frac{3}{2}} l_{cross} \quad (1)$$

$$l_p = \frac{L - d_{core}}{2} \quad (2)$$

With these parameters, we established the octapod aspect ratio L/D to denote the particle sizes.

Next, we proceeded to syntheses of octapod NCs by following protocols reported by our group^{17,25} with minor modifications. In detail, in a three-neck flask 60 mg of CdO, 6 mg of CdCl₂, 3 g of tri-*n*-octylphosphine oxide (TOPO), 290 mg of octadecylphosphonic acid (ODPA), and 80 mg of hexylphosphonic acid (HPA) were degassed for one hour at 130°C under stirring. The solution was then heated up to 350°C under nitrogen flow. When the solution became transparent ($\approx 260^\circ\text{C}$) 2.5 ml of anhydrous tri-*n*-octylphosphine (TOP) were injected in the flask. Once the temperature reached 350°C, a previously prepared mixture of the pre-synthesized Cu_{2-x}Se seeds in 500 μl of TOP and 620 μl of S precursor (32 mg/ml solution in TOP) were quickly injected in the mixture. The reaction was run for 10 minutes before the solution was fast cooled down to room temperature. When the temperature dropped below 100°C, 3 ml of anhydrous toluene were added to the resulting product. The colloidal dispersion was then washed twice



using a mixture of ethanol and methanol, and centrifuged to remove the excess of unbounded ligands.

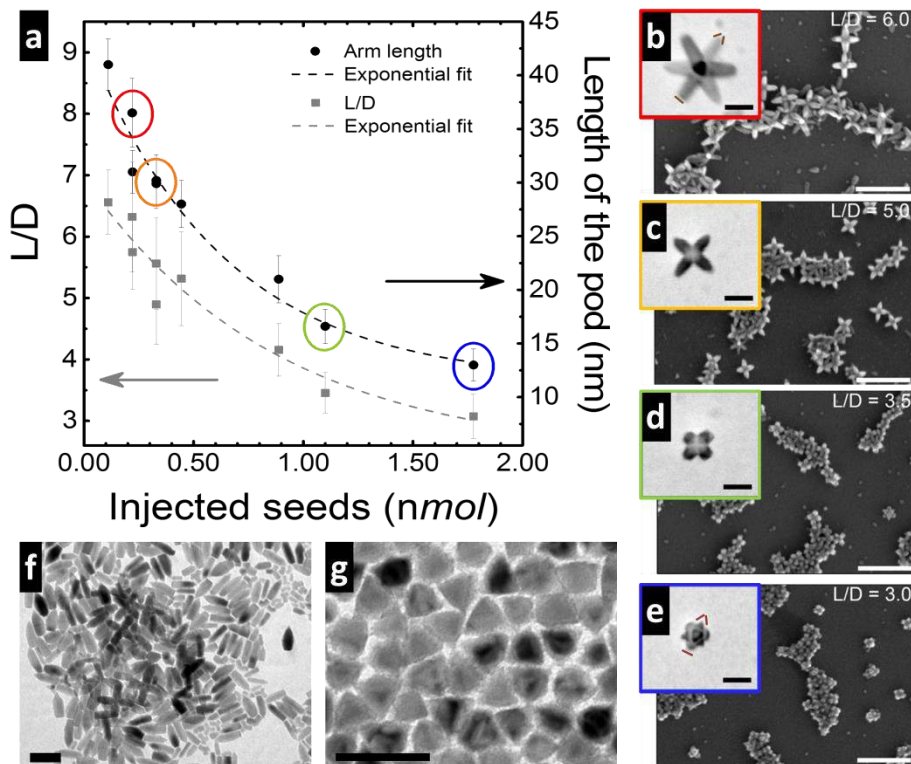


Figure 5. (a) Average octapod pod lengths, l_p , and aspect ratios, L/D , plotted as a function of the amount of injected Cu_{2-x}Se seeds; the error bars show the standard deviation. When the concentration of injected seeds is between 0.1 nmol and 2 nmol the resulting particles maintain the symmetry of octapods and their l_p and L/D decrease exponentially by incrementing the amount of seeds injected in the synthesis. The colour-framed points in the l_p curve correspond to the octapod batches selected for the analysis of their assembly. (b-e) High resolution scanning electron microscopy (HRSEM, see Appendix D.4) images of the selected octapods. In the insets, inverted HRSEM close views of single octapods. In (b) and (d) the alternation of flat and tapered tips is highlighted. Scale bars: 200 nm and 50 nm (insets). (f, g) TEM images showing the formation of rod-like or tetrahedral NCs obtained by using a seed concentration of 0.05 nmol and 2.7 nmol, respectively. Scale bars: 50 nm.



In order to tune the pod size, several syntheses were performed using different amounts of Cu_{2-x}Se seeds while keeping constant the amount of Cd and S precursors. In this way the quantity of CdS precursors available per seed was controlled. We found that the pod length l_p can be varied from 13.0 ± 1.5 nm, when using 1.8 nmol of Cu_{2-x}Se seeds, up to 41 ± 2 nm, when injecting 0.1 nmol of seeds. We observed that, instead, the thickness of the pods is not sensitive to the seed changes and it remains around 14 ± 2 nm. Thus, the octapod L/D aspect ratio can be tuned from 3.0 ± 0.4 up to 6.6 ± 0.5 . A detailed list of seeds amounts employed in the different syntheses and the estimated geometrical parameters, as well as a representative TEM image of the resulting particles is provided in Appendix A.

Interestingly, by plotting both l_p and L/D octapod parameters against the concentration of Cu_{2-x}Se seeds, it can be appreciated that they exponentially decrease when increasing the seed amount (Figure 5a). This behaviour is well described by equation (3).

$$y = Ae^{-x \cdot R_0} + y_0 \quad (3)$$

Where x represents the concentration of the seeds and y either l_p or L/D . The values for A , R_0 and y_0 found for the fittings are reported in Table 1.

Table 1. Specific values for the parameters of equation (3), that describe the changes on octapod aspect ratio with the seed concentration.

y	A	R_0	y_0
l_p	33 ± 2 nm	1.6 ± 0.4 nmol ⁻¹	11 ± 2 nm
L/D	4.5 ± 0.9	1.2 ± 0.6 nmol ⁻¹	2.4 ± 1.1

Such behaviour changes when injecting amounts of seeds out of the range showed in Figure 5a. The octapod shape becomes, indeed,



clearly compromised. For instance, CdS elongated structures are the dominant product of the synthesis for seed amount below 0.1 nmol (Figure 5f). This is an indication that the provided nucleation sites (seeds) are too dispersed to favour the growth of octapods. Instead, particles with a tetrahedral symmetry are formed when the Cu_{2-x}Se seeds concentration is increased above 1.8 nmol (Figure 5g).

The colour framed points in Figure 5a corresponds to the samples of octapods selected for further structural and optical characterization, as it will be described in the next paragraphs, and for surface analysis (Section 2.2). The same samples were also employed in planar self-assembly experiments, as reported in Chapter 3. The samples are named following their L/D and a colour has been assigned to each one to easily identify them. This colour code will hold through the present and next chapter: $L/D = 6$ is framed in red, $L/D = 5$ in orange, $L/D = 3.5$ in green and $L/D = 3$ in blue.

In order to evidence the morphology of the selected octapods series of high angle annular dark field - scanning transmission electron microscopy HAADF-STEM (see details in Appendix D.1.2) images at different tilting angles were collected in collaboration with Dr. R. Brescia, who also performed volume reconstructions for octapods with $L/D = 3$, $L/D = 3.5$ and $L/D = 6$, as shown in Figure 6. The analyses show that even the smaller octapods present eight pods with homogeneous length and triangular section. Also, they evidence that opposite pods have a flat and tapered tips, independently of their size, as reported for octapods with high aspect ratio¹⁸. These findings confirm that the mechanisms of growth and particle stabilization are not affected by the reduced amount of precursors available per single particle, since the facets exposed are the same.



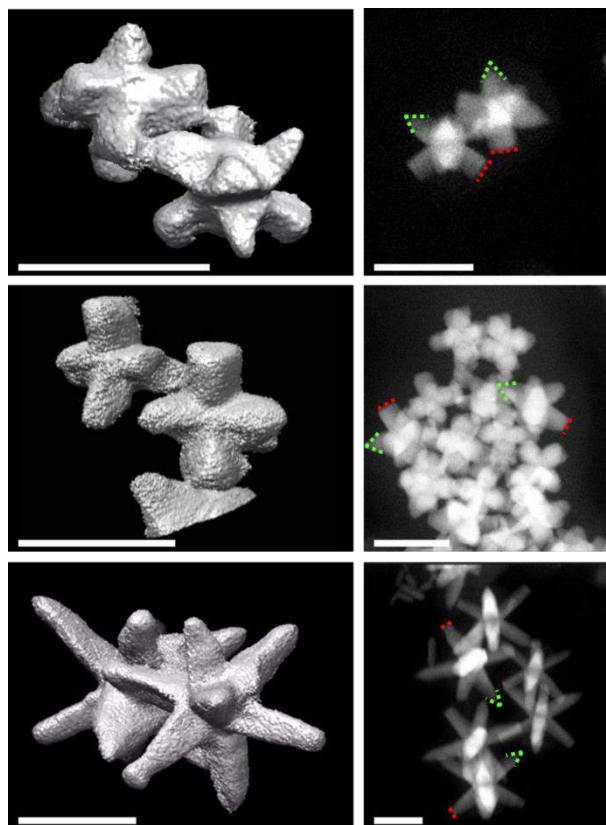


Figure 6. Volume reconstruction (left) and tilted HAADF-STEM images (right) of octapods with different L/D aspect ratio; from top to bottom, octapods with L/D of 3.0, 3.5 and 6.0. The images show the triangular section of the pods, as well as, their flat and tapered opposite tips from all the octapod sizes. In the HAADF-STEM images the flat tips are highlighted in red, while the tapered ones in green. Scale bars: 50 nm.

XRD characterization of the selected octapods, conducted in collaboration with S. Marras (details in Appendix D.5), confirmed that the particles are formed by a CdSe core with a sphalerite lattice, deriving from the cation exchange of the Cu_{2-x}Se seeds¹⁷, and by CdS pods with a wurtzite structure, as can be observed from the collected patterns in Figure 7. As it was expected, the relative intensity of CdS signals increased with the pod length, and it covers completely the signal coming from the CdSe core in the octapods with high aspect ratio.



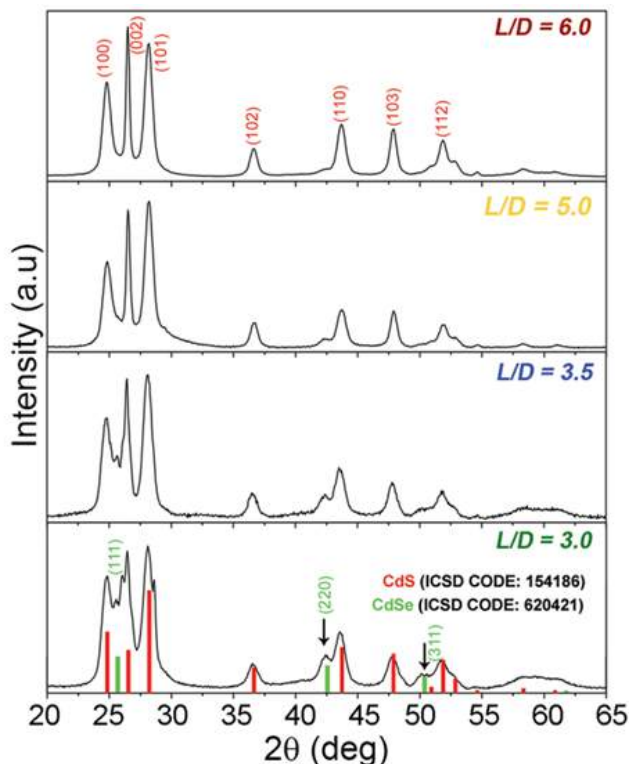


Figure 7. XRD patterns collected from samples with different L/D . The vertical lines are the reference used for wurtzite CdS (in red) and sphalerite CdSe (in green).

Overall, these results demonstrate that acting on the number of nucleation sites, by changing the concentration of Cu_{2-x}Se seeds, does not affect the structure of the octapods, but only the length of their pods.

In order to evaluate the impact of the changes of octapod size on their photoluminescence (PL), we recorded the PL spectrum from all the selected particles and from the CdSe core-like NCs (see Appendix D.6 for details about the acquisition of the spectra). The later were synthesized through the standard octapods synthesis protocol using a seed concentration of 1.8 nmol and without the addition of S precursor. As a result, the Cu_{2-x}Se seeds undergo only cation exchange without pod growth. The resulting NCs are faceted



CdSe cuboctahedra with an average diameter of 14 ± 3 nm (Figure 9b) and a sphalerite phase, as confirmed by XRD (Figure 8c).

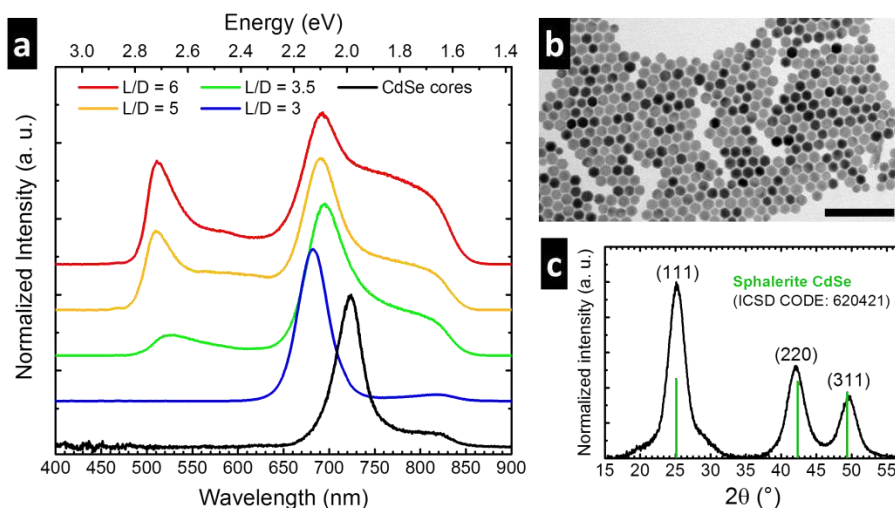


Figure 8. (a) PL spectra of octapods NCs with different aspect ratio. The emission from the CdSe cores is also included. (b-c) TEM image (b) and XRD pattern (c) collected from the synthesized CdSe NCs. In the spectra, the rise of the peak at 510 nm is ascribed to the emission of the CdS pods, while the peak at longer wavelengths can be related to a shifted CdSe core emission (originally located at ca. 723 nm), due to tensile strain introduced by the lattice mismatch with the CdS pods. The broad peaks around 600 nm and 800 nm can be referred to surface defects in CdS and CdSe respectively. Scale bar: 100 nm.

Figure 8a shows the emission of CdSe cores with a main PL peak at 723 nm, typical of this sphalerite phase²⁸. Also, there is a less pronounced peak around 810 nm. From octapods with a low aspect ratio (L/D of 3.0), the main peak of the seeds suffers a blue-shift to 682 nm and, when the pods grow longer the position of this peak shifts to ca. 690 nm. This can be attributed to the stress accumulated in the CdSe due to the CdSe – CdS lattice mismatch. An explanation to this observations is that a compressive strain is generated by the growth of short CdS pods, which results in a modified bandgap, and thus, in an emission blue shift. On the contrary, when longer CdSe pods are grown, the formation of



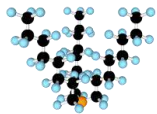
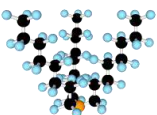
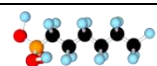
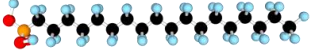
dislocations inside the CdS structure becomes the thermodynamically favoured route for stress relaxation, partially removing the strain from CdSe, and thus moving the emission to longer wavelengths²⁹. Additionally, three other peaks can be individuated in the spectra collected from octapods with higher L/D aspect ratio. There is a sharp peak at ca. 510 nm which is ascribed to the CdS emission from the pods³⁰ and, coherently, its intensity grows with the aspect ratio of the NCs. The broad shoulder around 590 nm might be related to surface defects in the CdS, like S vacancies, that act as recombination points³¹. The last peak, observed at ca. 800 nm is also present in the CdSe cores and it could be ascribed to non-exchanged Cu or CdSe surface defects.

2.2 Surface Analysis of Branched Colloidal Nanocrystals with Different Sizes

With the tight control over pod-length achieved with the current synthesis of octapods, which was described in the previous section, we performed a detail analysis of the particle surface following their different aspect ratios. In order to assess a surface ligand distribution and elucidate their potential role in NCs self-assembly (Chapter 3), we used Attenuated Total Reflection Fourier Transform Infrared Spectroscopy (ATR-FTIR, see Appendix D.7.1). The choice of using FTIR technique instead of quantitative nuclear magnetic resonance (NMR) was due to technical reasons: i) the acquisition of reference NMR spectra from unbounded ligands encountered several drawbacks due to their lack of solubility in a common solvent. This was the case of ODPA that was found to be soluble only in tetrahydrofuran (THF), a solvent in which octapods with high aspect ratio are not well dispersed; and ii) NMR requires concentrated (ca. 30 mM – 50 mM) and stable samples. In our case, octapods do not form stable suspension at such high concentration.



Table 2. Phosphorous-based ligands used in all the syntheses of octapods. A ball and stick model of each ligand is also included with the H, C, P and O atoms represented by cyan, black, orange and red, respectively.

	Sketch	Number of CH ₃	Number of CH ₂	Ratio $\frac{\# CH_2}{\# CH_3}$	Ratio $\frac{\# P}{\# CH_3}$
TOP		3	21	7:1	1:3
TOPO		3	21	7:1	1:3
HPA		1	5	5:1	1:1
ODPA		1	17	17:1	1:1

As described in Section 2.1, four different surfactants are employed in the synthesis of octapods: TOP (tri-*n*-octylphosphine), TOPO (tri-*n*-octylphosphine oxide), HPA (hexylphosphonic acid) and ODPA (octadecylphosphonic acid), see Table 2. They are all formed by a polar head containing a phosphorous atom and by apolar alkyl chain(s), three in the case of TOP and TOPO, and one for HPA and ODPA.

At first, we collected the FTIR spectra from the pure ligands described in Table 2. The results are shown in Figure 9. They were used as a reference for the analysis of the selected octapods, prior to self-assembly. The as-synthesized octapods are named here “native”.

From these spectra two main regions of interest can be identified: i) between 2750 cm⁻¹ and 3000 cm⁻¹ (CH_n stretching of alkyl chains) and ii) between 850 cm⁻¹ and 1250 cm⁻¹ (fingerprints of P-O stretching)³². The main differences among the ligands, in their FTIR spectra, is the relative intensities of the peaks located in the mentioned regions.



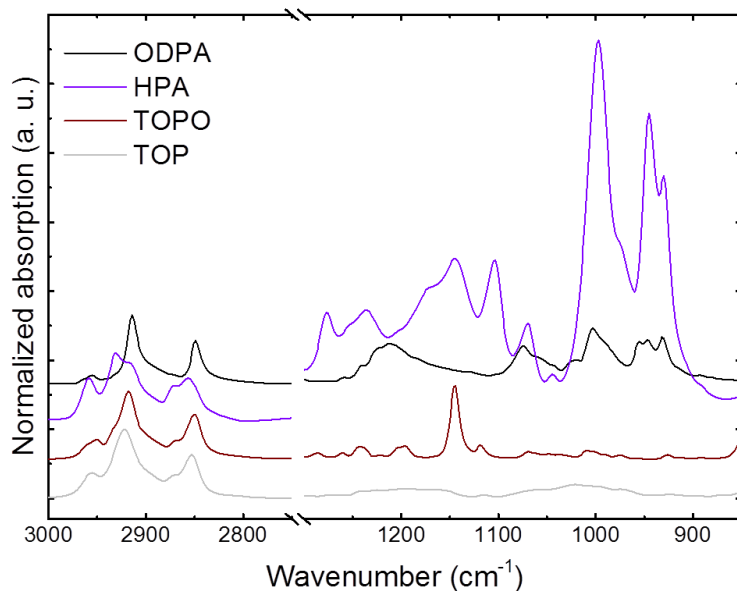


Figure 9. FTIR spectra collected from the pure ligands employed in the octapods syntheses (TOP, TOPO, HPA and ODPA). The peaks in the region between 3000 cm^{-1} and 2750 cm^{-1} correspond to the absorption of the CH_n stretching modes, while the peaks in the region between 1250 cm^{-1} and 850 cm^{-1} are from the absorption of the P-O modes.

The spectrum from pure TOP is dominated by the CH_n stretching signals, as it does not own P-O moieties; TOPO presents also a sharp peak at 1144 cm^{-1} , related to its $\text{P}=\text{O}$ moiety with an intensity comparable to the CH_n stretching signals. ODPA and HPA present both several signals in the region at lower wavenumber. In the case of ODPA, the intensities of the peaks in this region are comparable to those due to the CH_n stretching vibrational modes. Instead, the spectrum of HPA is dominated by the absorption from P-O moieties. This difference between the two acids is ascribed to the length of their alkyl chain. Both molecules owns, indeed, one P-O(H) moiety that absorbs at 850 cm^{-1} - 1250 cm^{-1} . However, ODPA molecules have 18 CH_n moieties that contributes to the absorption at high wavenumbers, while HPA only 6 CH_n .



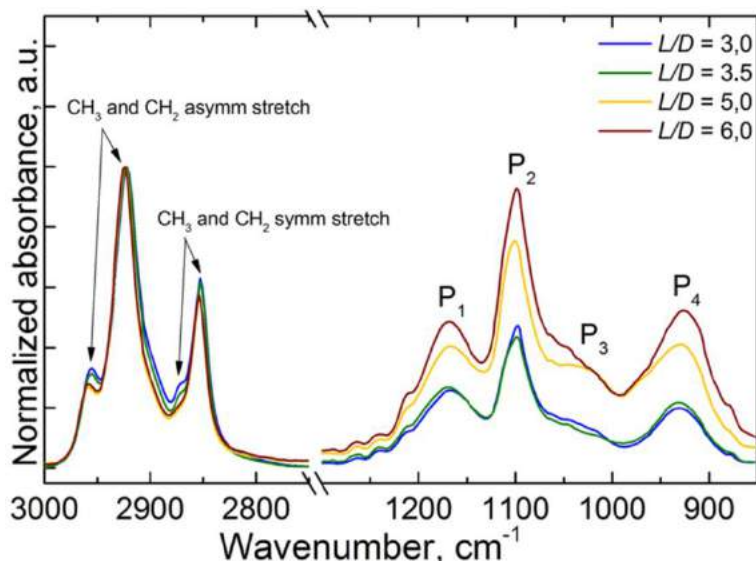


Figure 10. FTIR absorption spectra of octapods with different sizes. The assignment of P_n peaks identified in the spectra is explained in the main text.

Next, we proceeded to collect the IR absorption spectra for the native octapods with different aspect ratios. The signal was recorded from dry samples prepared by drop casting 2 μl of NCs dispersions in toluene directly on the ATR crystal. The nanometric dimensions of the particles ensured an intimate contact with the crystal, favouring the acquisition of spectra with low signal-to-noise ratio. The results obtained are shown in Figure 10. The analysis of the bound ligands on the octapod surface was carried out considering the two regions described above for the pure ligands. In the CH_n stretching region four peaks are identified:

- 2957 cm^{-1} CH_3 asymmetric stretching;
- 2923 cm^{-1} CH_2 asymmetric stretching;
- 2872 cm^{-1} CH_3 symmetric stretching (shoulder);
- 2854 cm^{-1} CH_2 symmetric stretching.

Also, in the region containing the fingerprints of P-O stretching modes, four main peaks were identified by following similar analysis



reported in literature³² and using the spectra from the pure ligands (Figure 9) as references:

- P_1 at 1167 cm^{-1} P=O stretching from acids;
- P_2 at 1100 cm^{-1} P=O stretching from TOPO and HPA;
- P_3 at 1054 cm^{-1} (broad shoulder) P=O from acids;
- P_4 at 926 cm^{-1} P-OH stretching from acids.

As it was expected, the similarities among the four spectra confirm that the overall ligand shell is formed by the same species, independently of the length of the pods, since all the particles were synthesized with the same type and amount of ligands. However, two types of surface can be identified:

- Short-pod family, composed by octapods with $L/D = 3.0$ and $L/D = 3.5$, with intense peaks related to CH_3 asymmetric and symmetric stretching modes in the region at high wavenumber and less intense peaks in the region at low wavenumber, that corresponds to the P-O stretching modes (P_n);
- Long-pod family, composed by octapods with $L/D = 5.0$ and $L/D = 6.0$, for which the intensity of the CH_3 asymmetric peak is reduced compared to the short-pod family, the CH_3 symmetric one is not observed, and the peaks related to the P-O stretching modes are enhanced.

The observed reduction of the peak intensities related to CH_3 modes, compared to the CH_2 ones, from octapods with high aspect ratio, is an indication that these particles are coated with a thicker ligand shell. In order to better visualize this increment in the chain length, the ratio R_{CH_n} as defined by equation (4) was introduced and evaluated for each octapod aspect ratio.



$$R_{CH_n} = \frac{Area_{asymmetric\ CH_2\ peak}}{Area_{asymmetric\ CH_3\ peak}} \quad (4)$$

The areas of the peaks in equation (4) were evaluated by deconvolution of all the four peaks related to CH_n stretching modes in Figure 10. Figure 11 shows the calculated values as a function of the particles aspect ratio L/D . It shows the increment of R_{CH_n} when increasing the pod length of the particles.

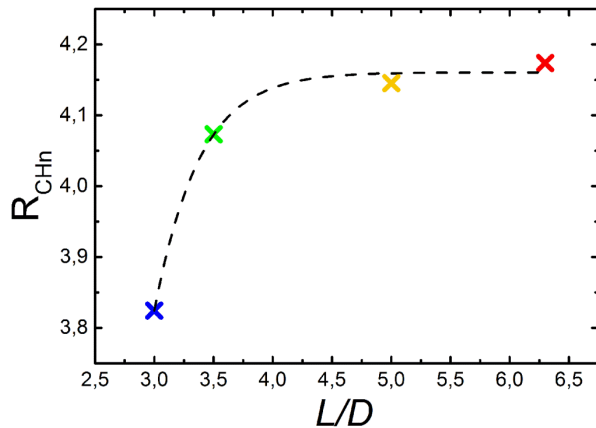


Figure 11. R_{CH_n} values calculated for octapods with different aspect ratio following (4). R_{CH_n} , i.e. the weight of CH_2 absorption over CH_3 , increases with the size of the octapods following a saturation behaviour. The increment indicates that the ligand shell covering NCs with longer pods is thicker than the one present on shorter pods. The dashed line is a guide for the eyes.

This observation indicates that there is an increment in the content of ODPa ligand in the surface coating. The ODPa molecule owns the longest alkyl chain among the ligands employed in the octapod synthesis. Also, in its unbounded state, ODPa is the only ligand that does not show a recognisable peak related to the CH_3 symmetric stretching (Figure 9), as it is also observed from octapods with high aspect ratio (Figure 10).

On the other hand, the change in the intensity of the peaks related to the P-O stretching modes observed in the FTIR spectra from octapods with a low aspect ratio suggests that their (thinner)



ligand shells are TOP-rich. As pointed out in the discussion relative to Figure 9, the TOP molecules contribute only in the CH_n region of the absorption spectra, given their lack of P-O moieties. Relative abundance of TOP in the ligand shell would thus result in an intensified absorption in the CH_n region compared to the P-O region, as it is observed from the particles with $L/D = 3.0$ and $L/D = 3.5$.

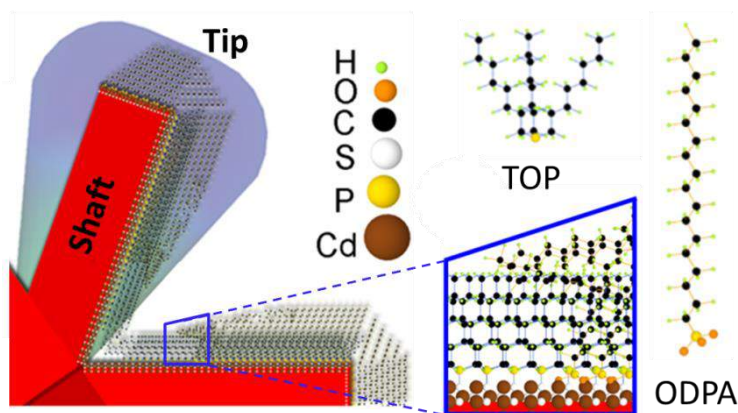


Figure 12. Sketches depicting the cone-like distribution of the ligands around the shafts of the octapods. The ligand shell is TOP-rich near the core, while the ODPA amount increases along the pod. In the sketch only TOP and ODPA are shown for clarity, but also TOPO and HPA should be present in the ligand shell.

It appears, moreover, that passing from octapods with a low aspect ratio of $L/D = 3.0$ to those with an $L/D = 6.0$, the increment in thickness of the ligand shell is not uniform along the pod length. Indeed, the identical faceting of the shafts of octapods with different L/D (Figure 6) eliminates any enthalpic origin to the preferential bounding of ODPA to longer pods. In addition to this, the steric hindrance created by the geometry of the pods near the core could explain a lack of ODPA on the initial portion of the shaft, due to the limited space provided for such large molecule to be adsorbed in this region. Hence, while the pods grow longer, their surface becomes more accessible to ODPA, which becomes abundant along the pod length. The thickness of the resulting



ligand shell on the shafts, thus, could assume a cone-like distribution with a thinner TOP-rich region near the core and a thicker ODPA-rich portion toward the tip, as illustrated in the sketch in Figure 12.

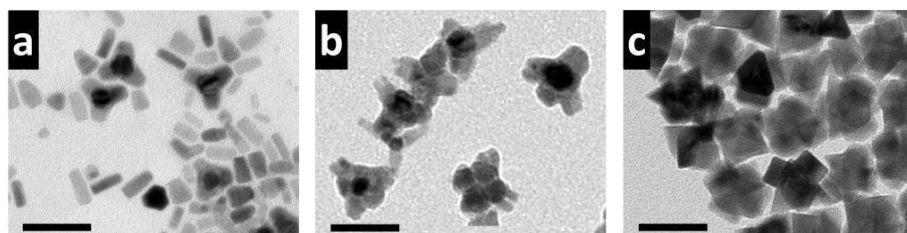


Figure 13. TEM images of the NCs obtained modifying the mixture of surfactants in the synthesis of octapods with L/D of 5.0. (a) Without HPA, the main products of the synthesis are small tetrapods and CdS rods with flat tips and low aspect ratio. (b) Without ODPA inhomogeneous particles with more than four pods are produced. (c) A reduction of the TOP amount, from 3.62 ml to 1.12 ml, produces particles with $L/D = 2.6$, instead of the expected $L/D = 5.0$. The particles show enlarged pods (ca. 20 nm thick) and strong faceting, with the tapered tips departing directly from the core. Scale bars: 50 nm.

Finally, in order to experimentally validate the proposed cone-like distribution of ligands along the pod length of the particles, a set of octapods syntheses was carried out changing the amount of ligands employed. The syntheses were performed keeping the amount of seeds constant (0.3 nmol, as for $L/D = 5.0$) and modifying the surfactants as follows:

- Complete removal of HPA ligand from the synthesis: In this case, the products of the synthesis are small tetrapods and rods NCs (Figure 13a). In the tetrapod geometry the pods are less crowded and more accessible to ODPA along all their length. Moreover, the reduced aspect ratio of the CdS structures formed is the result of strong facet stabilization/covering that prevents Cd and S precursors to



reach the surface of the existing NCs, favouring nucleation of new particles.

- Complete removal of ODPA ligand from the synthesis: In this case, irregular particles with several pods of different length are obtained (Figure 14b). The absence of ODPA allows for nucleation on all the $\{1\ 1\ 1\}$ facets of the CdSe cores, but the mixture of TOP, TOPO and HPA is not passivating the growing pods effectively, and thus it results in an inhomogeneous pod growth. Interestingly, in this sample, both the flat tips and the tapered tips are observed. The pods terminated by tapered tips, moreover, appear to be longer and with multiple termination, as if the growth on this family is that fast that, on the same $\{1\ 1\ 1\}_{\text{CdSe}}$ facet, multiple pods nucleate and grow at the same time.
- Strong reduction of the TOP content (from 3.12 ml to 1.12 ml): In this case, small and irregular octapod-like NCs with a strong faceting are obtained (Figure 14c). In this situation the registered pod thickness of $D = 20 \pm 4\ \text{nm}$ is significantly larger than the largest one observed for octapods synthesized with the standard technique ($D = 16 \pm 2\ \text{nm}$ in the $L/D = 5.0$ sample). Also, the family of pods with tapered tips is essentially limited to the tips themselves, with really reduced shafts length. This proves the fundamental role of TOP in stabilizing the shafts of the pods, favouring the growth along the $\langle 0\ 0\ 0\ 1 \rangle$ direction.



2.3 Conclusions and Outlook

In this chapter we have described the fine control achieved over the size of a class of branched NCs with an octapod geometry. This was obtained modifying only the number of Cu_{2-x}Se seeds injected in the synthesis. The NCs preserved their octapod shape in reactions carried out with an amount of seeds comprised between 0.1 nmol and 2 nmol. In this range the length of the pods can be effectively tuned between 40 nm and 13 nm, as it decreases exponentially with the number of seeds. Detailed morphological and structural characterization of the NCs confirmed that all the particles are formed by a sphalerite CdSe core and eight wurtzite CdS pods. Such pods, independently on their length, owns a triangular section, with the shafts terminated by $\{1\ 0\ 1\ 0\}$ planes, four tapered tips terminated by $\{1\ 0\ 1\ \bar{1}\}$ facets and four flat tips formed by a $(0\ 0\ 0\ 1)$ plane. We also revealed that the ligand coverage of the pod shafts, in the synthesized octapods is not to uniform, and we propose a model based on a cone-like distribution with longer molecules near the tips and shorter ones closer the octapod core. The availability of branched NCs with different dimensions along with their detailed characterization, including their surface ligand coverage, will enable a deeper investigation of their role in the assemblies. This will be detailed in the next Chapter.

2.4 Acknowledgements

The work presented in this Chapter was possible thanks to the collaboration of Dr. R. Brescia, who helped us with the morphological characterization of the NCs via HAADF-STEM imaging and volume reconstruction; and S. Marras, who supported the XRD characterization. The author would like also to



acknowledge Prof. V. Lesnyak for his precious help with the synthesis of the Cu_{2-x}Se NCs.

2.5 References

- 1 Blaak, R., Mulder, B. M. & Frenkel, D. Cubatic phase for tetrapods. *The Journal of Chemical Physics* **120**, 5486-5492, doi:10.1063/1.1649733 (2004).
- 2 Goodman, M. D. *et al.* Self-Assembly of CdTe Tetrapods into Network Monolayers at the Air/Water Interface. *ACS Nano* **4**, 2043-2050, doi:10.1021/nn1002584 (2010).
- 3 Mishra, N. *et al.* Continuous Shape Tuning of Nanotetrapods: Toward Shape-Mediated Self-Assembly. *Chemistry of Materials* **28**, 1187-1195, doi:10.1021/acs.chemmater.5b04803 (2016).
- 4 Miszta, K. *et al.* Hierarchical self-assembly of suspended branched colloidal nanocrystals into superlattice structures. *Nature Materials* **10**, 872-876, doi:10.1038/nmat3121 (2011).
- 5 Qi, W. *et al.* Ordered Two-Dimensional Superstructures of Colloidal Octapod-Shaped Nanocrystals on Flat Substrates. *Nano Letters* **12**, 5299-5303, doi:10.1021/nl302620j (2012).
- 6 Qi, W. *et al.* Phase diagram of octapod-shaped nanocrystals in a quasi-two-dimensional planar geometry. *The Journal of Chemical Physics* **138**, 154504, doi:10.1063/1.4799269 (2013).
- 7 Arciniegas, M. P. *et al.* Self-Assembly of Octapod-Shaped Colloidal Nanocrystals into a Hexagonal Ballerina Network Embedded in a Thin Polymer Film. *Nano Letters* **14**, 1056-1063, doi:10.1021/nl404732m (2014).
- 8 Sutter, E. *et al.* In situ microscopy of the self-assembly of branched nanocrystals in solution. *Nature Communications* **7** (2016).



- 9 Taniguchi, Y. *et al.* Programmed Self-Assembly of Branched Nanocrystals with an Amphiphilic Surface Pattern. *ACS Nano* **11**, 9312-9320, doi:10.1021/acsnano.7b04719 (2017).
- 10 He, X. & Gao, L. Morphology and phase evolution of hierarchical architectures of cadmium sulfide. *The Journal of Physical Chemistry C* **113**, 10981-10989 (2009).
- 11 Cao, X., Zhao, C., Lan, X., Yao, D. & Shen, W. Rapid phosphine-free growth of diverse CdSe multipods via microwave irradiation route. *Journal of Alloys and Compounds* **474**, 61-67 (2009).
- 12 Bashouti, M. & Lifshitz, E. PbS Sub-micrometer Structures with Anisotropic Shape: Ribbons, Wires, Octapods, and HOLLOWED Cubes. *Inorganic Chemistry* **47**, 678-682, doi:10.1021/ic700706a (2008).
- 13 Wang, X., Xi, G., Liu, Y. & Qian, Y. Controllable synthesis of PbSe nanostructures and growth mechanisms. *Crystal Growth and Design* **8**, 1406-1411 (2008).
- 14 Ren, J. & Tilley, R. D. Preparation, self-assembly, and mechanistic study of highly monodispersed nanocubes. *Journal of the American Chemical Society* **129**, 3287-3291 (2007).
- 15 Cheong, S., Watt, J., Ingham, B., Toney, M. F. & Tilley, R. D. In situ and ex situ studies of platinum nanocrystals: growth and evolution in solution. *Journal of the American Chemical Society* **131**, 14590-14595 (2009).
- 16 Chou, S.-W. *et al.* Controlled growth and magnetic property of FePt nanostructure: cuboctahedron, octapod, truncated cube, and cube. *Chemistry of Materials* **21**, 4955-4961 (2009).
- 17 Deka, S. *et al.* Octapod-Shaped Colloidal Nanocrystals of Cadmium Chalcogenides via “One-Pot” Cation Exchange and Seeded Growth. *Nano Letters* **10**, 3770-3776, doi:10.1021/nl102539a (2010).



- 18 Brescia, R., Miszta, K., Dorfs, D., Manna, L. & Bertonni, G. Birth and Growth of Octapod-Shaped Colloidal Nanocrystals Studied by Electron Tomography. *The Journal of Physical Chemistry C* **115**, 20128-20133, doi:10.1021/jp206253w (2011).
- 19 Jana, N. R. Shape Effect in Nanoparticle Self-Assembly. *Angewandte Chemie International Edition* **43**, 1536-1540 (2004).
- 20 Liu, K., Zhao, N. & Kumacheva, E. Self-assembly of inorganic nanorods. *Chemical Society Reviews* **40**, 656-671 (2011).
- 21 Ye, X. *et al.* Morphologically controlled synthesis of colloidal upconversion nanophosphors and their shape-directed self-assembly. *Proceedings of the National Academy of Sciences* **107**, 22430-22435, doi:10.1073/pnas.1008958107 (2010).
- 22 Park, K. H., Jang, K. & Son, S. U. Synthesis, Optical Properties, and Self-Assembly of Ultrathin Hexagonal In₂S₃ Nanoplates. *Angewandte Chemie International Edition* **45**, 4608-4612, doi:10.1002/anie.200601031 (2006).
- 23 Saunders, A. E., Ghezelbash, A., Smilgies, D.-M., Sigman, M. B. & Korgel, B. A. Columnar Self-Assembly of Colloidal Nanodisks. *Nano Letters* **6**, 2959-2963, doi:10.1021/nl062419e (2006).
- 24 Castelli, A. *et al.* Understanding and Tailoring Ligand Interactions in the Self-Assembly of Branched Colloidal Nanocrystals into Planar Superlattices. *Nature Communications* **Under 1st revision**.
- 25 Kim, M. R. *et al.* Influence of chloride ions on the synthesis of colloidal branched CdSe/CdS nanocrystals by seeded growth. *ACS Nano* **6**, 11088-11096, doi:10.1021/nn3048846 (2012).



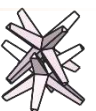
- 26 Deka, S. *et al.* Phosphine-free synthesis of p-type copper (I) selenide nanocrystals in hot coordinating solvents. *Journal of the American Chemical Society* **132**, 8912-8914 (2010).
- 27 Saldanha, P. L. *et al.* Generalized One-Pot Synthesis of Copper Sulfide, Selenide-Sulfide, and Telluride-Sulfide Nanoparticles. *Chemistry of Materials* **26**, 1442-1449, doi:10.1021/cm4035598 (2014).
- 28 Hernández-Calderón, I. in *II-VI Semiconductor Materials and their Applications Optoelectronic Properties of Semiconductors and Superlattices* (ed Maria C. Tamargo) Ch. IV, 113-170 (Taylor & Francis Inc., 2002).
- 29 Chen, X., Lou, Y., Samia, A. C. & Burda, C. Coherency Strain Effects on the Optical Response of Core/Shell Heteronanostructures. *Nano Letters* **3**, 799-803, doi:10.1021/nl034243b (2003).
- 30 Collins, R. Mechanism and defect responsible for edge emission in CdS. *Journal of Applied Physics* **30**, 1135-1140 (1959).
- 31 Xiao, Q. & Xiao, C. Surface-defect-states photoluminescence in CdS nanocrystals prepared by one-step aqueous synthesis method. *Applied Surface Science* **255**, 7111-7114 (2009).
- 32 Ahmed, S. & Ryan, K. M. Centimetre scale assembly of vertically aligned and close packed semiconductor nanorods from solution. *Chemical Communications*, 6421-6423, doi:10.1039/B914478A (2009).





3 Planar Self-Assembly of Branched Colloidal Nanocrystals

The self-assembly of anisotropic NCs have been envisioned as an effective bottom-up technique to realize structures with properties and geometries otherwise unattainable¹⁻⁵. However, the control of the resulting assembly cannot be disjointed from a deep understanding of the interactions that takes place in the system^{1,2,6-8}. As pointed out in Section 1.2.1, the morphology of the NCs (size and shape) and the ligand-mediated interactions are fundamental in determining the final structure obtained by self-assembly. Tuning such parameters, thus, provides an effective tool to control the geometry of the superlattices^{9,10}. Such control has allowed to obtain ordered structures, even from complex systems, such as hexagonal nanoplates¹¹ or tetrahedral NCs¹². In this Chapter it will be shown how the interplay of morphology-related and ligand-mediated interaction is able to direct the assembly of highly anisotropic NCs such as octapods. Thanks to the advancement in the synthesis of such NCs and the improved understanding of their surface coating presented in Chapter 2, a wide library of particles with different



sizes and known ligand distribution is now available. We will address their assembly behaviour in Section 3.2, by using an interfacial self-assembly technique that is described in Section 3.1. A theoretical analysis of the experimental finding is provided in Section 3.3, to confirm the role of the experimental model formulated for the ligands distribution on the octapod assemblies. A last section in this chapter is dedicated to the experimental changes on the particle ligands by using ligand exchange techniques, to explore new configurations from a single type of particle.

The present chapter is based on our work recently submitted article to Nature Communications [18].



3.1 Interfacial Self-Assembly Technique

In 2010 Murray's group established an assembly technique, that exploits the immiscibility between two liquids to create a tri-phasic liquid-liquid-air system and produce self-assembled 2D membranes of NCs¹³. In such technique an aliquot of NCs suspension is cast over an immiscible and denser liquid sub-phase, that acts as a substrate. The NCs suspension is, then, allowed to evaporate slowly. In order for the technique to be effective, the particles must be insoluble in the liquid substrate. In this way, while the NCs solvent evaporates, the particles that are confined in the liquid layer are forced to arrange themselves in a single layer. Once the solvent evaporation is complete, a floating membrane of NCs is left at the liquid-air interface. The advantages of using such technique are numerous: i) forcing the system toward a compact structure, it ensures the activation of short-range particle-particle interactions that allows to study their effect on the NC self-assembly; ii) limiting the system to a bidimensional structure, it maximizes the in-plane interactions among NCs and it reduces the sources of disorder given by out-of-plane misalignment; iii) the fluidity of the substrate enhances the particles rotational and translational freedom, avoiding the formation of coffee stains and producing homogeneous membranes; and iv) the floating membrane can be collected employing any kind of solid substrates, in response to the requirement of the subsequent analysis.

In our study we implemented this technique by using diethylene glycol (DEG) as the sub-phase and hexane as NCs solvent. In a typical experiment (Figure 2) Teflon wells with a volume capacity of 4.5 ml are filled with 2 ml of DEG. 20 μ l of sonicated suspensions of NCs in hexane, with concentration between 0.5 nM and 10 nM, are then drop cast on the top of the DEG. Next, the wells are closed for 10 min with a glass slide. After that, the system is opened to allow complete evaporation of the hexane layer. The



yellow-coloured floating membrane formed on the DEG is then collected on the desired substrates (carbon-coated TEM Cu grids or type-p Si substrates of 5 x 5 mm²). The remaining DEG layer below the NCs membranes was removed either via 48h vacuum drying or annealing at 130°C on a hotplate.

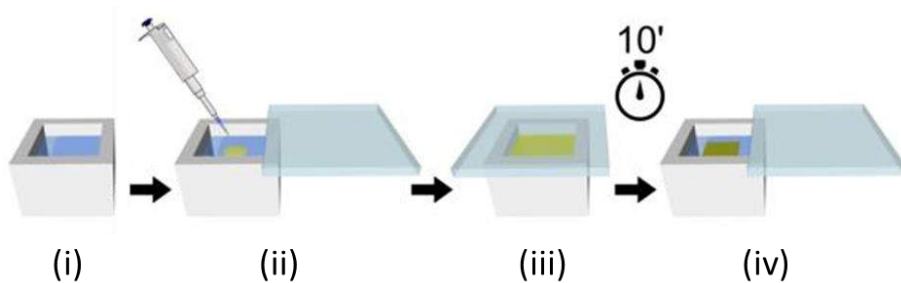


Figure 2. Sketch representing the interfacial self-assembly technique employed for the assembly of octapods into planar superlattices. On a diethylene glycol (DEG) substrate (i) few microliters of a dispersion of NCs in hexane are drop (ii), the system is closed with a glass slide for ten minutes (iii) and, once the cover is removed, a self-assembled floating membrane is formed at the centre of the well (iv). The layer can then be fished with different substrates.

3.2 Planar Self-Assembly of Native Octapods

With the described assembly approach 2D membranes were prepared using the four octapods with different sizes synthesized and characterized as described in Chapter 2. That is particles with aspect ratios L/D of 3.0, 3.5, 5.0 and 6.0. The concentration of NCs in the starting hexane dispersion was initially kept constant at 5 nM. The assembly procedure brought all the samples to create micrometre-scaled compact islands, where octapods form uniform monolayers; the eventual defects are segregated at the edges of the membranes (Figure 3a-d). The organization of the particles inside this monolayer, was found to be strongly dependent on their size, as highlighted in the closer SEM views in Figure 3e-h.



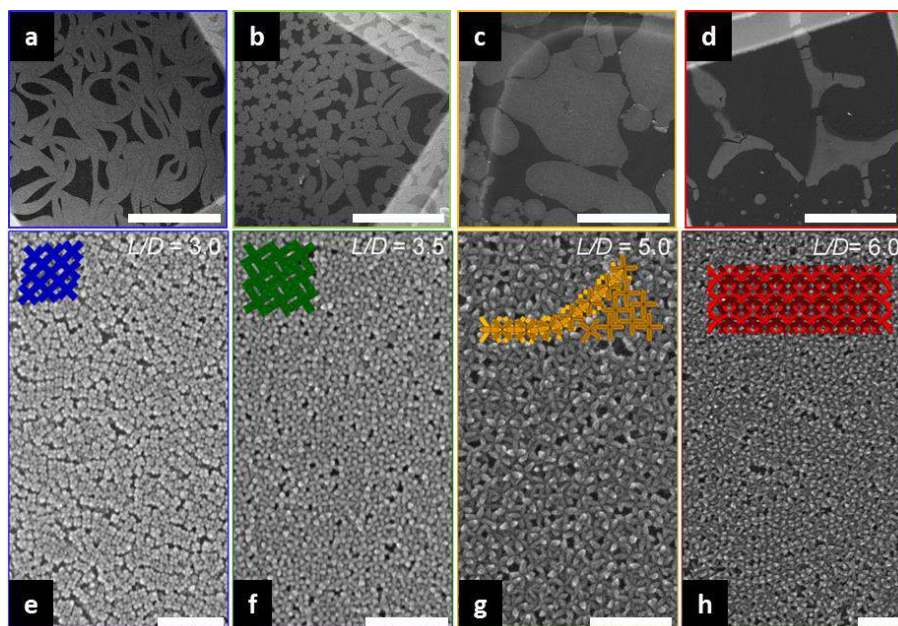


Figure 3. Low (a-d) and high (e-f) HRSEM images of the self-assembled 2D membranes of octapods from suspensions in hexane at 5 nM. The sketches in (e-f) shows the dominant architecture of octapods in their assemblies. Scale bars: (a-d) 20 μm ; (e-h) 200 nm.

In detail, octapods with shorter pods ($L/D = 3.0$ and $L/D = 3.5$) form extended islands where all the NCs touch the substrate with four pods, giving a cross projection under EM investigation. In both cases, the membranes are composed by a mosaic of small ordered domains formed by up to 50 NCs (Figure 3e,f). In the case of $L/D = 3.0$ these domains present a geometry (Figure 4a), which is similar to the rhombic lattices predicted by W. Qi et. al for smaller octapods induced by drop cast by mean of only geometrical consideration¹⁴. The assembly of octapods with $L/D = 3.5$, instead, resembles the square lattices predicted by the same authors (Figure 4b). In our membranes such ordering is limited by skewed particles that rotate from the ideal configuration and achieve a tip-to-tip contact with the neighbouring octapods, as evidenced in the embedded sketches in Figure 4b. This configuration of octapods create a pocket between two closer octapods.



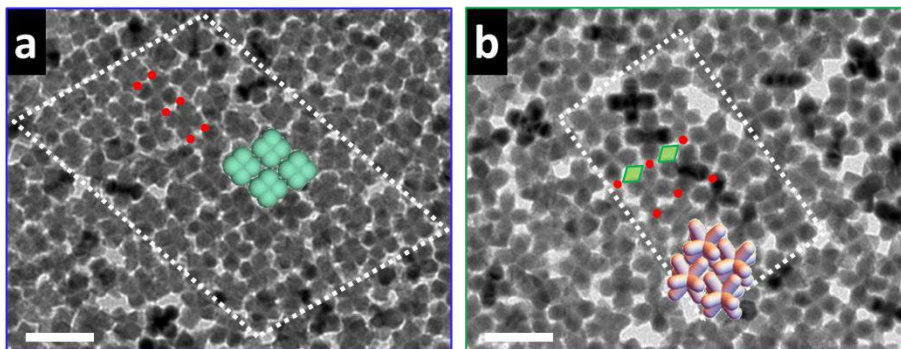


Figure 4. Close TEM views of ordered domains (framed in white) generated by the interfacial self-assembly of octapods with $L/D = 3.0$ (a) and $L/D = 3.5$ (b) prepared from NCs suspension in hexane at 5 nM. The embedded sketches illustrate the observed configuration of octapods. In (a), the sketch is adapted from [22]. Octapods with $L/D = 3.5$, are rotated and exhibit an enhanced tip-to-tip contact, as highlighted by red dots in the image. This twisted configuration brings to the formation of empty pockets among neighbouring octapods, reducing the density of the membrane. Two of such pockets are evidenced in green in (b). Scale bars: 50 nm.

While such pocket is interesting to host a second, convex particle, as it will be discussed in Chapter 4, its formation cannot take place in a system that is driven purely by entropy minimization. Thus, the favourable tip-tip interaction observed from the octapods can be originated by the cone-like distribution of the ligands wrapping their pods, as it will be discussed further in Section 3.3.

Remarkably, when the octapod aspect ratio is increased to an $L/D = 5.0$ we observe the formation of linear arrays made of interlocked particles. This peculiar organization is typical of octapods, as it has already been reported to occur in solution^{5,15}, in the coffee stain region of a 2D assembly on solid substrate¹⁶ and, as detailed in Chapter 5, inside a polymer matrix¹⁷. Along with this octapod arrangement, there are also domains of particles with a cross-projection (Figure 3g). An example of such mixed domains is shown in Figure 5a.



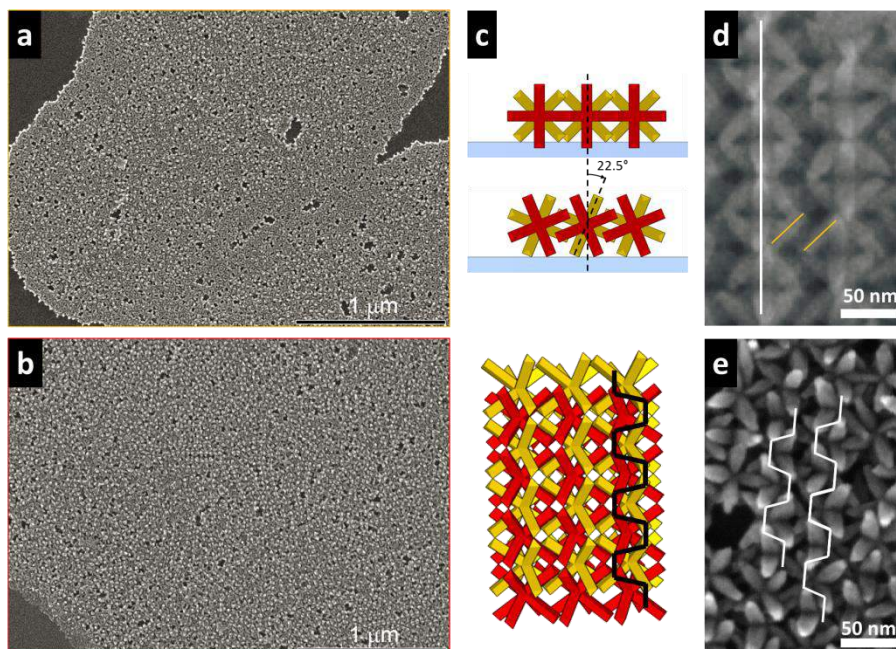


Figure 5. Low magnification HRSEM images of the planar superlattices formed by octapods with $L/D = 5.0$ (a) and $L/D = 6.0$ (b) prepared from a suspension at 5 nM. They show the increased amount and length of chains in the membranes by increasing the octapod aspect ratio. The sketches in (c) exemplify the rotation of chains at the DEG interface in order to avoid the immersion of any pod in the polar substrate. The bottom sketch depicts the packing of three rotated chains and it highlights the zig-zag profile given by the top-protruding octapod tips. (d-e) Closer HRSEM views of the chains observed in 3D (d) and 2D (e) superlattices. The linear profile offered by the top-protruding tips (white line) and the parallel alignment of the pods belonging to different chains (orange line) are also highlighted in the images. Panel (d) is adapted from [5].

By increasing further the aspect ratio of the NCs to an $L/D = 6.0$, the interlocking chains become the dominant configuration in their planar superlattices. The abundance of linear structures and the contextual reduction of four-pod-standing octapods allows for chain-chain interactions that result in their tight packing. This gives to the assembled membranes the aspect of a “fabric” (Figure 5b-d). The octapod interlocking to form chains is similar to that observed in previous works of our group, but



produced under different experimental conditions^{5,16,17}. In the chains of interlocked octapods that form their 3D superstructures, the pods of particles belonging to neighbouring chains are aligned in parallel and a top view of the chains resulted in an alternated sequence of octapods touching the substrate with four and two tips (“four-two” configuration showed in Figure 5d). In our planar superlattices, the chains undergo a rotation of $\pi/8$ around their main axis, giving a zig-zag aspect to the line formed by the top-protruding pods (Figure 5c,e). This tilting of the chains is attributed to the presence of the DEG sub-phase. If, indeed, the chains would organize in the four-two configuration observed in 3D superstructures, it will bring the two bottom protruding pods inside the DEG, which is energetically disfavoured given the lipophilic coating of the NCs. The rotation of the chain prevents this immersion in the polar substrate (Figure 5c).

The formation of chains have been demonstrated in previous works to be a consequence of an attractive interaction among octapods⁵. In order to understand if such interactions is also influenced by octapod density, we conducted the same experiments at different concentrations of particles. Thus, we proceeded with the same experiment described above (Section 3.1) for the formation of the planar superlattices using an octapod suspension at 5 nM, but working with the concentrations of 2 nM, and 10 nM. The results are shown in Figure 6.

The assembly of octapods with $L/D = 3.5$ was found to be unresponsive to the changes in the initial concentration of NCs. In any of the tested concentrations, the particles touch the substrate with four pods and create small ordered domains with square lattice limited by skewed particles in tip-to-tip contact. In contrast, particles with higher aspect ratios exhibit changes in their organization depending on the amount of NCs present in the starting solution.



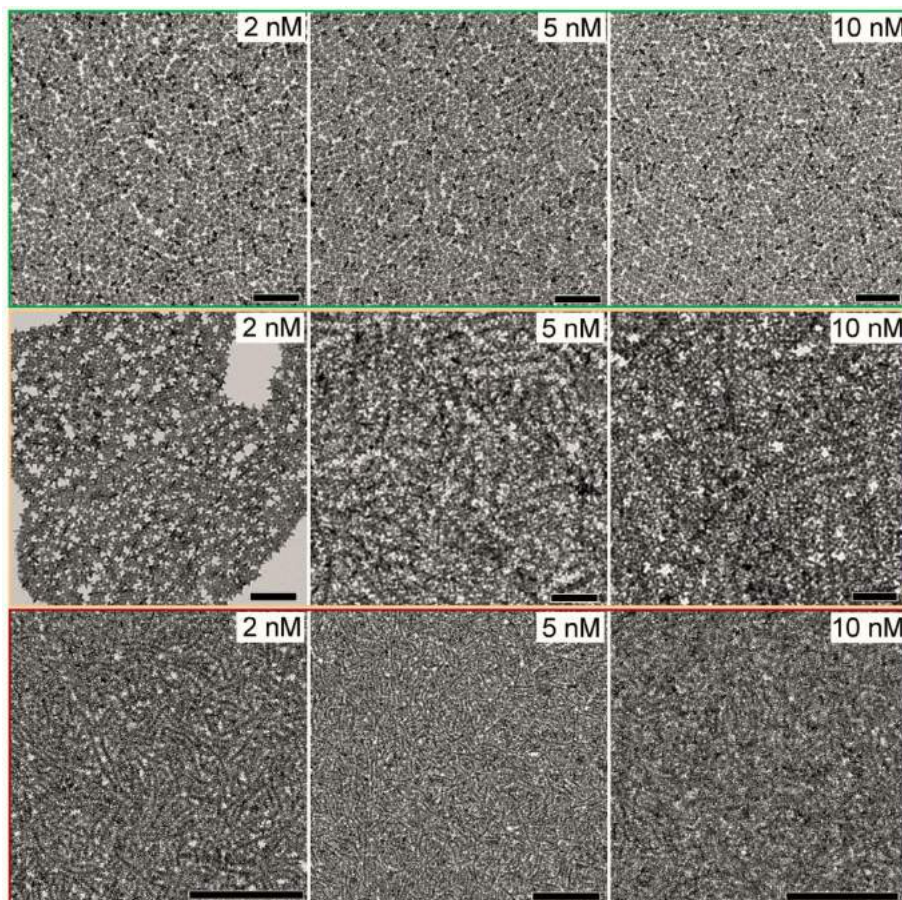


Figure 6. TEM images of the planar superlattices formed by octapods with different sizes and prepared from suspensions at different concentration. From top to bottom, $L/D = 3.5$, $L/D = 5.0$ and $L/D = 6.0$. Scale bars: 200 nm (for the panels of octapods with L/D of 3.5 and 5.0); 500 nm (for the panels of octapods with L/D of 6.0).

Octapods with $L/D = 5.0$, indeed, show a concentration threshold for the formation of chains between 2 nM and 5 nM. As already discussed, these particles are able to form sparse linear structures when assembled from 5 nM dispersions. Reducing the concentration of NCs and, thus, octapod interactions, the interlocking of octapods is prevented. Starting from dispersion at 2 nM the octapods assume the cross-projection configuration observed for particles with smaller aspect ratios. When the concentration is instead increased



up to 10 nM the octapods are still able to form chains, but the linear structures are less extended than those observed from suspension at 5 nM. This is attributed to an oversaturated condition that limits the out-of-plane mobility of the octapods in the superlattice. Finally, when octapods with $L/D = 6.0$ are employed, the ability to create interlocked structures remains over the entire spectrum of concentrations investigated. However, as happened for the sample with $L/D = 5.0$, the oversaturated conditions induced by using a suspension at 10 nM reduce the average length of the assembled chains.

3.3 Role of the Native Anisotropic Ligand Shell on the Self-Assembly of Octapods

The experimental results presented in the previous section evidenced that the octapods arrangement in their assemblies is strongly affected by their aspect ratio. In the case of octapods with low aspect ratio, it appears that there is a preferential tip-tip attractive interactions. Interestingly, previous theoretical analysis of the octapod assemblies have , identified a tip-to-tip attraction, acting together a core-core attraction, as the cause of octapods interlocking⁵. It is, thus, reasonable to assume that, independently of the size, the NCs experience a tip-tip interaction during their self-assembly. The presence of a thicker organic region near the tips, indeed, could explain the preference toward tip-tip contact as a way to maximize the overlapping between the ligand shells of two closer octapods.

In order to test this hypothesis, numerical simulations of the planar self-assembly of octapods when covered by such anisotropic ligand shell were conducted by Prof. J. de Graaf. Details of the analysis is here briefly described¹⁸. Prof. J. de Graaf implemented a standard isothermal-isobaric (*NPT*) Monte Carlo method, where the inorganic core of the NCs was approximated with four intersecting



spherocylinders (Figure 7a). Each spherocylinder is formed by a cylinder (length $L' = L - D$ and diameter D) capped with two hemispheres with diameter D . In order to simulate the excluded volume interactions, a hard overlap potential was given to this core, while a “soft” (short-ranged) potential was employed to simulate the interaction between ligand shells. This potential was divided in two sections: around the hemispherical tips the potential is constant, while along the shaft the interaction strength decreases while approaching the core of the particle (Figure 7b). Note that the model considers only tip-to-tip and shaft-to-shaft interactions, since tip-to-shaft interactions are not observed experimentally.

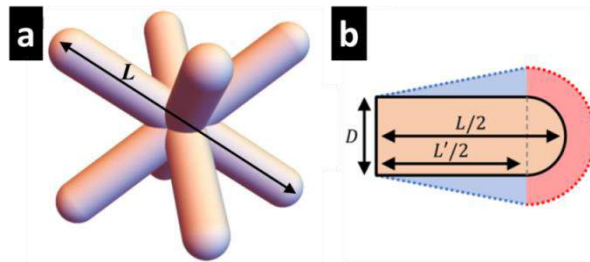
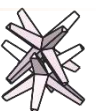


Figure 7. (a) Octapod model employed in the numerical simulations for the theoretical analysis of their assemblies considering the effect of the particle ligand coating. (b) A profile of the pod “soft” interaction potential. The red region represents where the tip-tip interaction is effective, while the blue one accounts for shaft-shaft interaction. In the sketches the dimensions employed for the simulations are also highlighted.

In order to reproduce the experimental conditions, where the NCs are confined in a thin layer of hexane over the DEG substrate, the centres of the particles were forced to stay all in the same plane. Moreover, in order to mimic the evaporation of the solvent, an external constant pressure was imposed to the systems. The simulations were performed for five different dimensions of octapods, namely $L/D = 3.0$, $L/D = 4.0$, $L/D = 5.0$, $L/D = 6.0$ and $L/D = 7.0$. The tip-tip strength of interaction, ε_T , and the shaft-shaft one, ε_S , were varied between $-5 k_B T$ and $5 k_B T$ and the



applied pressure between $0.17 \cdot 10^{-2} Nk_B T L^{-3}$ and $44.2 \cdot 10^{-2} Nk_B T L^{-3}$. The complete results are collected in Appendix B.

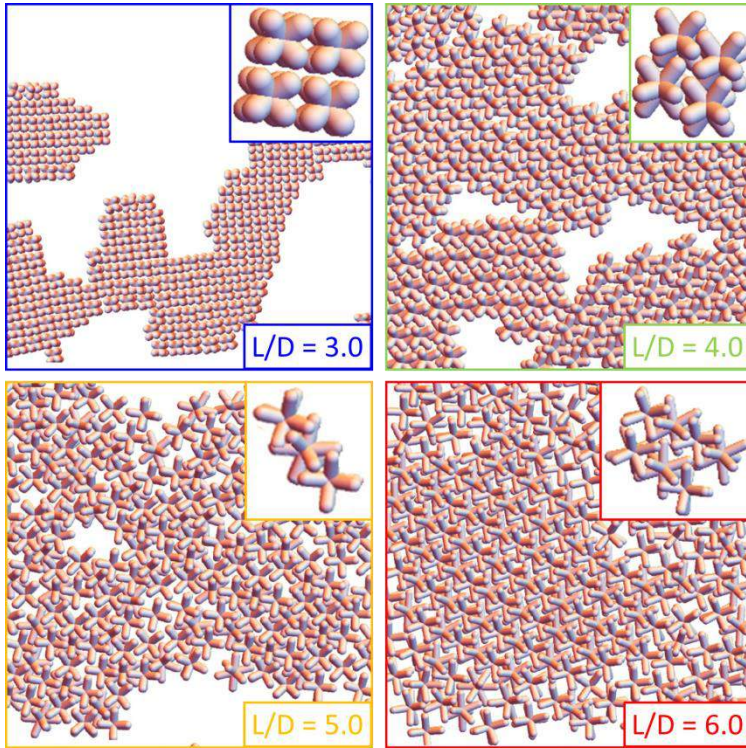


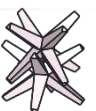
Figure 8. Results of the numerical simulations of planar self-assembly of octapods with different aspect ratios carried out imposing a ligand-mediated interaction potential with mild tip-tip attraction ($\epsilon_T = -1 k_B T$) and shaft-shaft repulsion ($\epsilon_S = 4 k_B T$). Theoretical analysis conducted by Prof. J. de Graaf.

The simulations show that, under the conditions employed, self-assembly of octapods is obtained only when at least one of the imposed interaction is attractive. When both tip-tip interaction and shaft-shaft interaction are absent (only entropic interaction) or repulsive, disorganized aggregates are formed. In particles with $L/D = 3.0$ and $L/D = 4.0$, moreover, the shafts are too small to have a real impact on the assembly, so the final structures present ordered superlattices only if the tip-tip interaction is attractive. The geometry formed, in these cases, is a skewed square lattice that



favours tip-tip contact and is not affected by changes in the pressure applied on the system (Figures B1-B4). For octapods with $L/D = 5.0$ superlattices with an interlocking configuration started to appear, accompanied by ordered and disordered domains of octapods standing on four pods, in agreement with the experimental results. The interlocking becomes clearer if the aspect ratio of the particles is raised to $L/D = 6.0$, while it disappears if the pressure applied on the system is increased (Figures B5-B8). Interestingly, the interlocked configuration is obtained, for both $L/D = 5.0$ and $L/D = 6.0$, when a shaft-shaft repulsion ($\varepsilon_S = 4 k_B T$) is added to a mild tip-tip attraction ($\varepsilon_T = -1 k_B T$). In Figure 8 are reported the results of the simulations for such values of ε_S and ε_T for particles with $L/D = 3.0 - 6.0$. The presence of a repulsive shaft-shaft interaction in the system suggests that the forces acting on that region are not dominated by van der Waals attraction, but other ligand-mediated interactions are at work.

Chains of interlocked NCs, however, were not the only ordered structures observed in simulations carried out on octapods with $L/D \geq 5.0$. Indeed, modifying the intensity of ε_T and ε_S , other ordered structures were found. For example, if the shaft-shaft repulsion is reduced from the conditions that brings to the formation of chains ($\varepsilon_S = 2 k_B T$) a different interlocked structure is formed which is extended over two dimensions (Figure 9a). If an attractive shaft-shaft interaction is imposed ($\varepsilon_S = -3 k_B T$) domains of octapods forming ballerinas' ballets are formed (Figure 9b). This structure was found to be the preferred one for particles with an attractive shaft-shaft interaction over a wide range of conditions (Figures B5, B7 and B9).



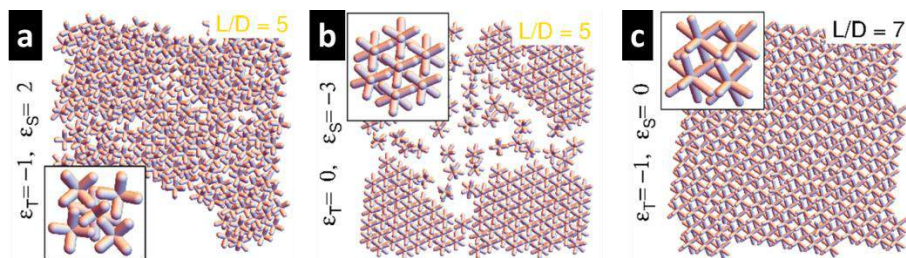


Figure 9. Collection of ordered structures obtained from simulations, but not observed in the 2D self-assembly of native octapods: interlocked 2D structures (a), ballerinas' ballet (b) and open square lattice (c).

Finally, the investigation of the assembly of octapods with an aspect ratio higher than the ones employed in experiments ($L/D = 7.0$) brought to the discovery of a new stable structure with square symmetry (Figure 9c and Figures B9-B10). This configuration is achieved when $\varepsilon_T < 0$ and under this condition the particles touch the substrate with four pods and are in tip-to-tip contact, forming an open structure.

The results of the simulations remarked the importance of ligand-mediated interactions and confirmed that the anisotropic distribution of surfactants on the pods of this class of branched NCs is responsible for their interlocking. Moreover, the prediction of other stable structures achievable by tuning the ligand-mediated interactions spurred the experimental investigation of the planar self-assembly with ligand exchanged particles, as detailed in the next section.

3.4 Self-Assembly of Ligand-Exchanged Octapods

Among the octapods of different sizes employed in Section 3.1, particles with $L/D = 3.5$ and $L/D = 5.0$ were selected for the study of the effect of a new ligand shell on their assemblies. The two octapod aspect ratio were selected for the following reasons: the assembly of octapods with $L/D = 3.5$ appeared, in the simulations,



to be insensible to the particle ligand coating; on the other hand octapods with $L/D = 5.0$ were selected because, being at the boundary between chains interlocking and cross-projection configuration, it is predicted to be the most sensitive toward changes in the ligand-mediated interaction potential.

Several ligands were tested: the four single ligands employed in the octapod synthesis (TOP, TOPO, HPA, ODPA), three thiols with different chain length (1-hexanethiol – HT, 1-dodecanethiol – DDT and 1-octadecanethiol – ODT) and oleylamine (OLAM). In order to perform the ligand exchange, three strategies were implemented: i) stripping with nitrosonium tetrafluoroborate (NOBF_4)¹⁹, ii) stripping with ethylenediamine (EDA)²⁰ and iii) ligand exchange via incubation with excess of surfactant. This latter procedure was carried out as follows: 300 μl of the new ligand was added to 300 μl of octapods in toluene ($[NPs] = 10 - 20 \text{ nM}$). The mixture was left overnight under stirring at 80°C. In the case of ODT, HPA, ODPA and TOPO, 300 μl of 0.1 mM solution in toluene were added to the octapods. The ligand exchanged particles were then cleaned from the unbound surfactants via two cycles of destabilization with methanol, centrifugation and re-dispersion in hexane.

The first approach, NOBF_4 stripping, resulted in the etching of the particles (Figure 10a), while the procedure with EDA gave not-dispersible aggregates (Figure 10b). Overnight incubation at 80°C was found to be the most efficient protocol for these ligands, as confirmed by the FTIR analysis of the exchanged particle surfaces (Figure 10c). However, the exchange with ODT was found not complete, even after 24h of incubation. Also, ODPA and HPA exchanged octapods with an aspect ratio of $L/D = 5.0$ formed aggregates when dissolved in hexane, resulting impossible to perform properly the self-assembly experiments.



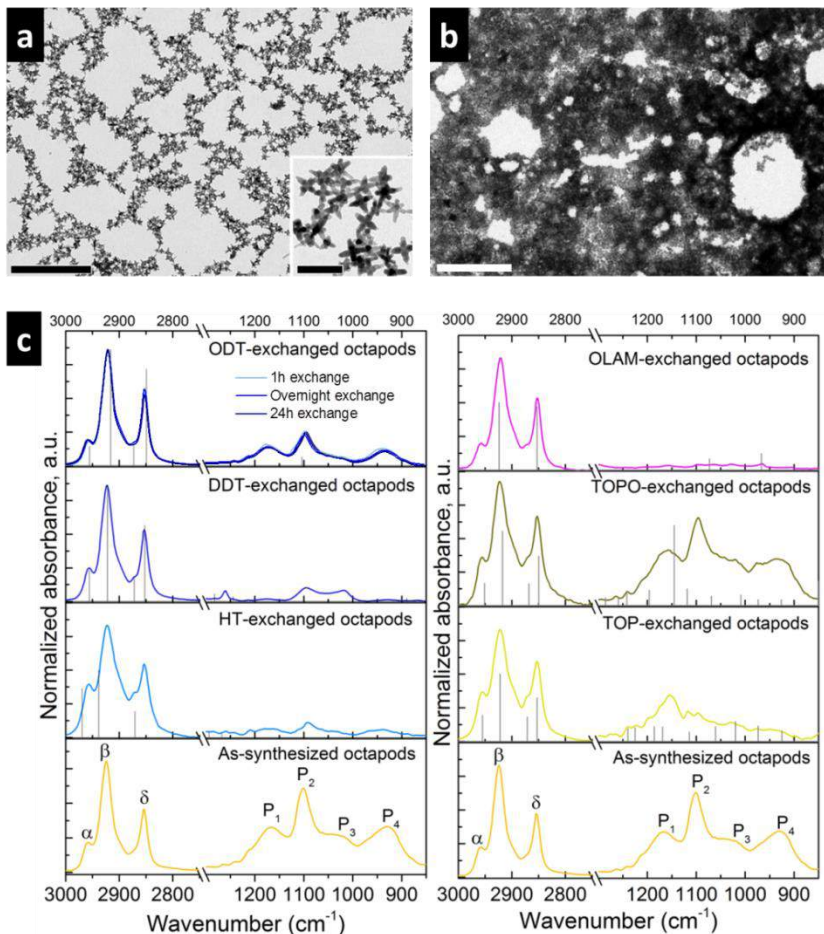


Figure 10. TEM images of octapods with $L/D = 5.0$ after DDT ligand exchange via stripping with NOBF_4 (a) and EDA (b). In the former case the particles are severely etched, while in the latter octapods form aggregates. (c) FTIR absorption spectra of the exchanged octapods ($L/D = 5.0$) incubated overnight at 80°C with excess of new ligands confirming the effectiveness of this procedure. The vertical grey lines in the spectra represent the positions and intensities of the absorption peaks of the unbound surfactants. HT, DDT and OLAM give an efficient ligand exchange, as the P_n peaks of the native shell are missing or show really reduced intensity. The ligand exchange with ODT is limited and it does not improve increasing the incubation time. Similarly, TOP and TOPO ligand exchanges are only partial. In the bottom panels of (c), where the absorption of octapods with native ligand shell is reported, α , β and γ refers to the peaks due to the absorption of CH_3 asymmetric stretching, CH_2 asymmetric stretching and CH_2 symmetric stretching respectively. Scale bars: (a) 500 nm, inset 100 nm; (b) 1 μm .



The efficient ligand exchange on octapods with $L/D = 5.0$ performed with HT, DDT and OLAM allowed to tune the overall ligand shell thickness, as demonstrated by the relative intensities of the CH_n stretching peaks and the R_{CH_n} ratio calculated for the different samples (Figure 11). The definition of R_{CH_n} is provided in Section 2.2, equation (4). The ligand shell formed by HT, a ligand that owns a short alkyl chain composed by 6 carbons (5 CH_2 and 1 CH_3), results in a R_{CH_n} significantly lower than that evaluated from the native octapods. Instead, by using DDT as surfactant (12 carbons, 11 CH_2 and 1 CH_3) it results in a R_{CH_n} value similar to the original ligand shell. OLAM, finally, is the ligand with the longer lipophilic tail, as it is formed by 18 carbons (15 CH_2 , 1 CH_3 and 2 $=\text{CH}$ whose contribution was not included in the calculation of R_{CH_n}). The particles covered with OLAM, thus, present a R_{CH_n} value superior to octapods covered by DDT or by the native ligand shell.

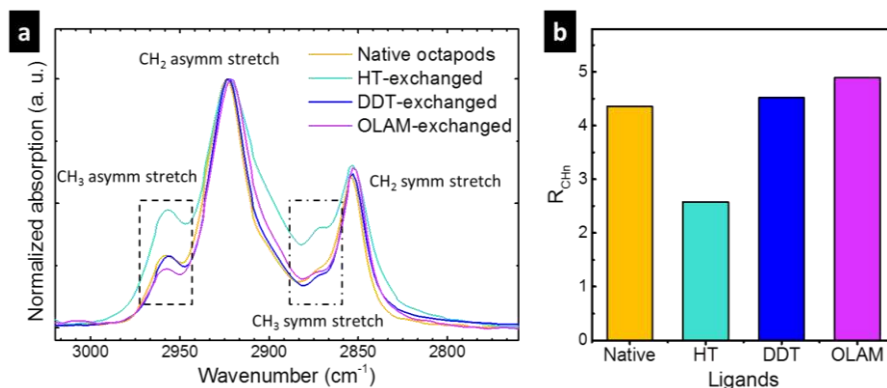


Figure 11. (a) FTIR absorption spectra in the region of CH_n stretchings of alkanes for octapods with $L/D = 5.0$ covered by their native ligand, and after ligand exchange with HT, DDT, OLAM. (b) The calculated R_{CH_n} for each ligand condition. Following the values of R_{CH_n} , it shows that the HT exchanged octapods are coated by a thinner ligand shell than the native ones, while the DDT gives a thickness similar to the original one. Finally, OLAM gives the thickest ligand shell.



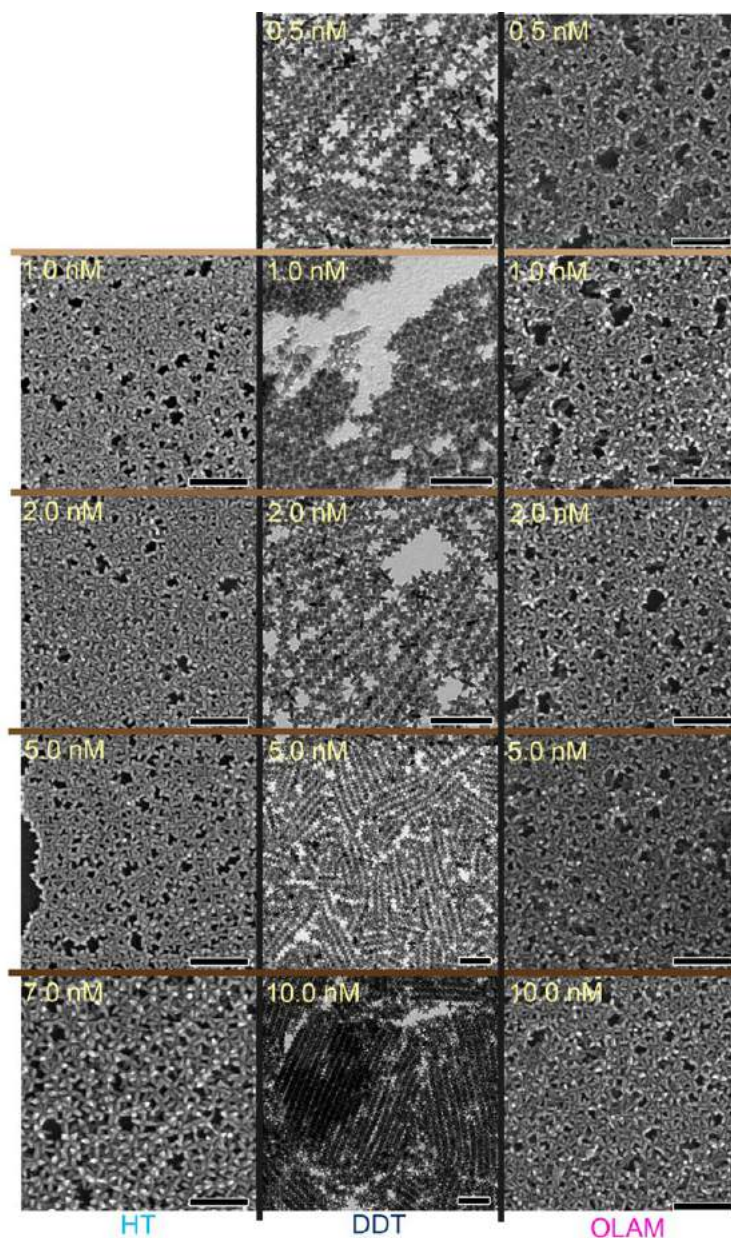


Figure 12. Collection of representative TEM and HRSEM images recorded from self-assembled membranes formed by octapods with $L/D = 5.0$ after ligand exchange with HT (left), DDT (centre) and OLAM (right) Each image is relative to a different concentration of NCs present in the starting hexane suspension. The assembly of the thiol-coated particles is sensitive to the concentration of octapods while particles coated with OLAM layer are not affected by the changes on octapod density. Scale bars: 200 nm.



Next, the effect of the changes on the ligand shell on the planar self-assemblies of the studied octapods were investigated in a wide range of concentrations for NCs with $L/D = 5.0$, spanning from 0.5 nM up to 10 nM. The realization of the self-assembled membranes was carried out employing the same interfacial technique reported in Section 3.1 and used for native octapods in Section 3.2. The results are shown in Figure 12.

Below a concentration of 7 nM, the presence of HT on the surface of octapods prevents the formation of chains (left column in Figure 12). At 7 nM short chains are found randomly dispersed in the superlattices. At concentration between 1 nM and 5 nM, octapods standing on four pods form dense planar superlattices. The disposition of the particles, even if lacking of long range order, resembles the binary square lattice reported in literature for octapods on a solid substrate and simulated without considering the ligand shell around the particles^{14,16}.

The retained ability to form interlocked linear assembly by HT-exchanged octapods suggests that the intensity of the tip-tip attraction and shaft-shaft repulsion (ϵ_T and ϵ_S as defined in Section 3.3) are not affected by the exchange. However, the effectiveness of these interaction is reduced, as they become relevant only when particles are closer due to the high concentration employed. This can be ascribed to the reduced thickness of the ligand coating, as the particles need to be closer to promote the overlapping of their ligand shell and experience the ligand-mediated interactions. On the other hand, a DDT-rich ligand shell resulted in the formation of chains at all the concentrations studied, from 0.5 nM to 10 nM. In particular, the chains are not immersed in a matrix of four-pods-standing particles, as it happens in the native octapods, but form dense packing of chains. This behaviour would suggest an improved effectiveness (longer cut-off distance) of the ligand mediated interactions with DDT coating compared to the native shell.



The presence of an OLAM-rich ligand coating on the octapod surface has a completely different effect than that observed from DDT. It indeed prevents the formation of chains, even at 10 nM. The octapods, at all concentrations, touch the substrate with four pods, forming a loose arrangement of particles. At low concentrations, by-products coming from the synthesis, like rods and bullets, fill the voids among octapods, instead of being segregated at the edges of the octapods domains. At higher concentrations, small domains of few particles exhibit a square lattice geometry^{14,16}. The absence of chains suggests that the OLAM suppresses the tip-tip attraction between particles. The concomitant absence of particles in ballerina's configuration proves that also the shaft-shaft interactions are not attractive. An OLAM ligand coating on octapod surface, thus, induces a non-interacting or repulsive shell around the NCs. This was verified carrying out analogous ligand exchange on particles with $L/D = 6.0$ and studying their self-assembly at 5 nM (Figure 13).

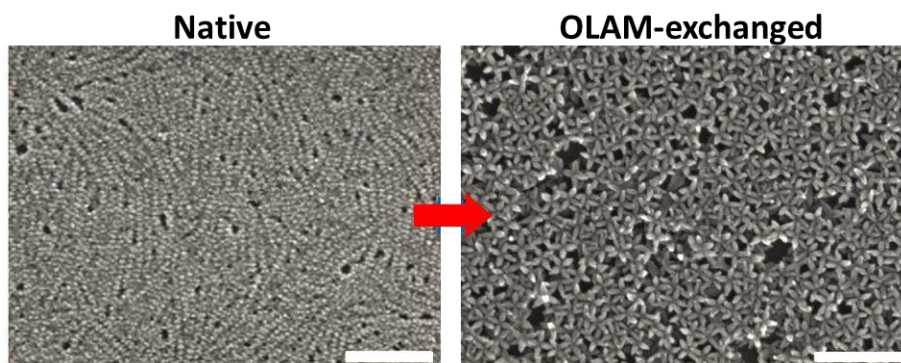


Figure 13. HRSEM images of self-assembled membranes formed by 5 nM dispersions of octapods with $L/D = 6.0$ covered by native ligand shell (left) and after OLAM exchange (right). OLAM-coating completely prevents the formation of chains. Scale bars: 500 nm (left) and 200 nm (right).

Also in this case, where chain formation had been found to be predominant in native octapods, the interlocking of particles is completely suppressed in favour of loose square lattices.



Finally, the effect of ligand exchange with TOP and TOPO on the 2D assembly of octapods with $L/D = 5.0$ was investigated (Figure 14). Even if such ligand exchanges were found to only partially modify the octapod ligand shell (Figure 10), the effect on the structure of the assembled membranes appears to be relevant (Figure 14).

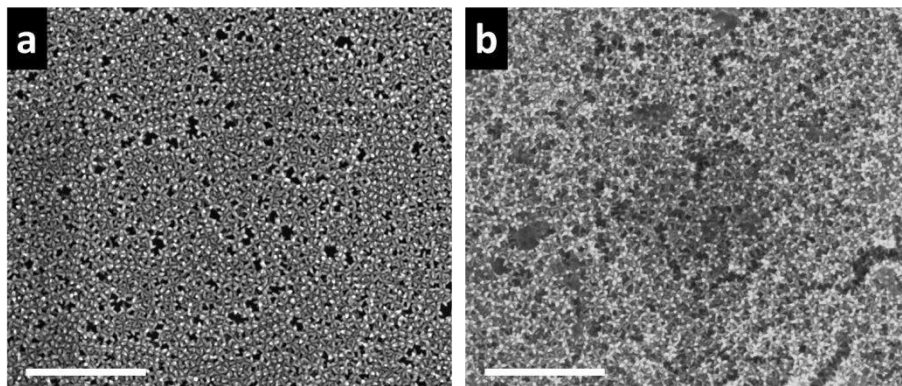


Figure 14. Representative HRSEM images of self-assembled membranes formed by 5 nM dispersions of $L/D = 5.0$ octapods with TOP (a) and TOPO (b) ligand coating. The TOP promotes the lateral packing of chains, as they form small ordered domains embedded in a matrix formed by octapods with cross-projection configuration. TOPO, on the other way, makes the assembly more chaotic, with the lack of chains of interlocked particles. Scale bars: 500 nm.

Self-assembled membranes from suspensions of TOP-exchanged octapods at 5 nM, are formed by chains in a matrix of four-pods-standing NCs, as it was observed from native octapods. However, the TOP ligand exchange seems to boost the alignment of chains, as packing of two or three parallel chains can be found in the membranes. The assembly of TOPO-coated octapods, instead, strongly differs from the structures formed by native particles. In this case, the NCs form dense monolayers where several octapods stand on one pod, assuming the ballerina's configuration. Even if the general assembly lacks of order, the presence of the ballerina's configuration is a clear indication of TOPO-induced shaft-shaft



attractive interaction, which has never been observed in the previous experiments.

Overall, these results show that coating a single type of octapods with different ligands is an effective way to tune the short-range ligand-mediated interactions occurring among the particles. Consequently, the architecture in their self-assemblies can be modified.

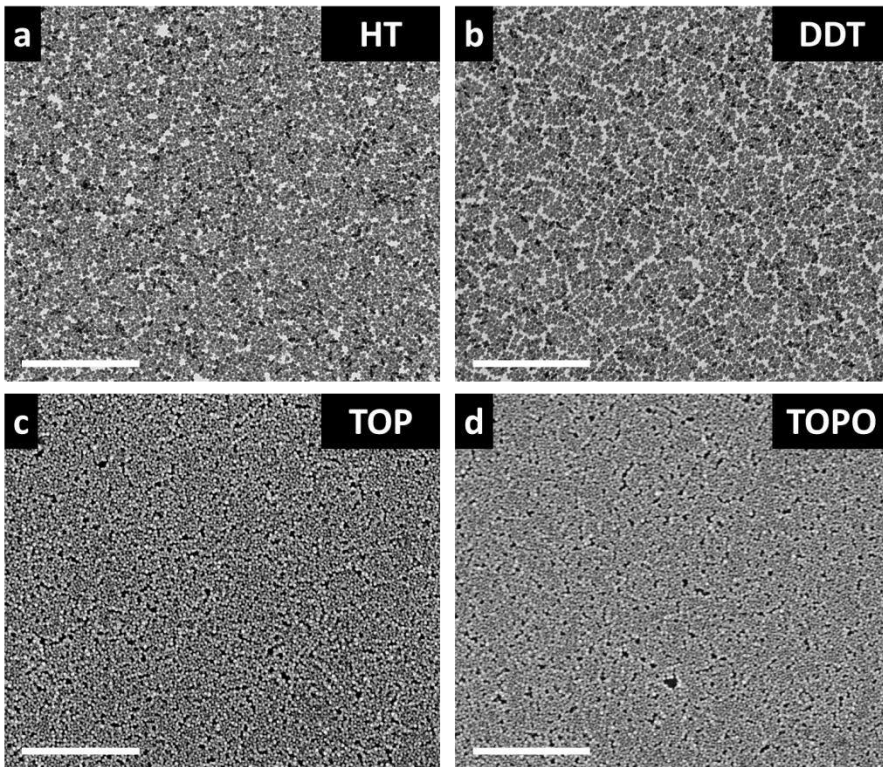


Figure 15. TEM and HRSEM images of self-assembled membranes formed by 5 nM dispersions of octapods with $L/D = 3.5$ and different ligand shell: HT (a), DDT (b), TOP (c) and TOPO (d). The particles do not undergo significant changes in their disposition, as all the octapods touches the substrate with four pods and there is not long range order. However HT and TOPO exchanged particles give denser packing, while the DDT forces the formation of small ordered domains. Scale bars: 500 nm.



Finally, in order to understand if the assembly of octapods with a low aspect ratio can also be sensible to their ligand coating, we studied particles with $L/D = 3.5$ after ligand exchange with HT, DDT, TOP and TOPO (Figure 15). The assembly experiments were conducted from NC suspensions at 5 nM. As it was suggested by the simulations, the changes in the ligand shell did not result in significant modifications of the assembled geometry of the particles in their planar superlattices. The octapods remain in a cross-like projection, forming extended membranes with small domains of square lattices. Note that HT and TOPO-exchanged octapods exhibited more compact domains than the other ligand-exchanged particles.

3.5 Conclusions and Outlook

The study of the planar self-assembly of branched NCs uncovered the fundamental role played by the anisotropic ligand shell in dictating their final geometry. By comparing the experimental data obtained with numerical simulations that considered the cone-like distribution of the surfactants, it allowed to identify the concomitant presence of ligand mediated tip-tip attraction and shaft-shaft repulsion as the driving force toward the formation of interlocked linear structures, the signature configuration of octapods. The role played by the ligand shell in the assembly of the NCs enabled to tune and control the structure of the formed membranes by ligand exchange. The formation of interlocked structures can, then, be prevented, hindered or favoured by the proper selection of ligand coating. Moreover the particles can be guided to acquire configurations not achievable when coated by native ligands, such as the ballerina's configuration.



3.6 Acknowledgements

The work presented in this Chapter was possible thanks to the collaboration of Dr. J. de Graaf, who conceived, performed and analysed the numerical simulations of the system. The author would like also to acknowledge Dr. L. de Trizio and Prof. V. Lesnyak for the useful suggestions about the different ligand exchange procedures.

3.7 References

- 1 Boles, M. A., Engel, M. & Talapin, D. V. Self-Assembly of Colloidal Nanocrystals: From Intricate Structures to Functional Materials. *Chemical Reviews* **116**, 11220-11289, doi:10.1021/acs.chemrev.6b00196 (2016).
- 2 Nie, Z., Petukhova, A. & Kumacheva, E. Properties and emerging applications of self-assembled structures made from inorganic nanoparticles. *Nature Nanotechnology* **5**, 15-25 (2010).
- 3 Lu, F., Yager, K. G., Zhang, Y., Xin, H. & Gang, O. Superlattices assembled through shape-induced directional binding. *Nature Communications* **6**, 6912, doi:10.1038/ncomms7912 (2015).
- 4 Singh, G. *et al.* Self-assembly of magnetite nanocubes into helical superstructures. *Science* **345**, 1149-1153, doi:10.1126/science.1254132 (2014).
- 5 Miszta, K. *et al.* Hierarchical self-assembly of suspended branched colloidal nanocrystals into superlattice structures. *Nature Materials* **10**, 872-876, doi:10.1038/nmat3121 (2011).
- 6 Grzelczak, M., Vermant, J., Furst, E. M. & Liz-Marzán, L. M. Directed Self-Assembly of Nanoparticles. *ACS Nano* **4**, 3591-3605, doi:10.1021/nn100869j (2010).



- 7 Singamaneni, S., Bliznyuk, V. N., Binek, C. & Tsymbal, E. Y. Magnetic nanoparticles: recent advances in synthesis, self-assembly and applications. *Journal of Materials Chemistry* **21**, 16819-16845, doi:10.1039/C1JM11845E (2011).
- 8 Bishop, K. J. M., Wilmer, C. E., Soh, S. & Grzybowski, B. A. Nanoscale Forces and Their Uses in Self-Assembly. *Small* **5**, 1600-1630, doi:10.1002/smll.200900358 (2009).
- 9 Quan, Z. & Fang, J. Superlattices with non-spherical building blocks. *Nano Today* **5**, 390-411 (2010).
- 10 Wang, Z. *et al.* Correlating Superlattice Polymorphs to Internanoparticle Distance, Packing Density, and Surface Lattice in Assemblies of PbS Nanoparticles. *Nano Letters* **13**, 1303-1311, doi:10.1021/nl400084k (2013).
- 11 Ye, X. *et al.* Competition of shape and interaction patchiness for self-assembling nanoplates. *Nature Chemistry* **5**, 466-473, doi:10.1038/nchem.1651 (2013).
- 12 Boles, M. A. & Talapin, D. V. Self-Assembly of Tetrahedral CdSe Nanocrystals: Effective “Patchiness” via Anisotropic Steric Interaction. *Journal of the American Chemical Society* **136**, 5868-5871, doi:10.1021/ja501596z (2014).
- 13 Dong, A., Chen, J., Vora, P. M., Kikkawa, J. M. & Murray, C. B. Binary nanocrystal superlattice membranes self-assembled at the liquid–air interface. *Nature* **466**, 474-477, doi:10.1038/nature09188 (2010).
- 14 Qi, W. *et al.* Phase diagram of octapod-shaped nanocrystals in a quasi-two-dimensional planar geometry. *The Journal of Chemical Physics* **138**, 154504, doi:10.1063/1.4799269 (2013).
- 15 Sutter, E. *et al.* In situ microscopy of the self-assembly of branched nanocrystals in solution. *Nature Communications* **7** (2016).
- 16 Qi, W. *et al.* Ordered Two-Dimensional Superstructures of Colloidal Octapod-Shaped Nanocrystals on Flat Substrates. *Nano Letters* **12**, 5299-5303, doi:10.1021/nl302620j (2012).



- 17 Arciniegas, M. P. *et al.* Assembly of Branched Colloidal Nanocrystals in Polymer Films Leads to Enhanced Viscous Deformation Resistance. *Nano Letters* **16**, 6154-6163, doi:10.1021/acs.nanolett.6b02371 (2016).
- 18 Castelli, A. *et al.* Understanding and Tailoring Ligand Interactions in the Self-Assembly of Branched Colloidal Nanocrystals into Planar Superlattices. *Nature Communications* **Under 1st revision**.
- 19 Dong, A. *et al.* A Generalized Ligand-Exchange Strategy Enabling Sequential Surface Functionalization of Colloidal Nanocrystals. *Journal of the American Chemical Society* **133**, 998-1006, doi:10.1021/ja108948z (2011).
- 20 Dai, M.-Q. & Yung, L.-Y. L. Ethylenediamine-Assisted Ligand Exchange and Phase Transfer of Oleophilic Quantum Dots: Stripping of Original Ligands and Preservation of Photoluminescence. *Chemistry of Materials* **25**, 2193-2201, doi:10.1021/cm304136a (2013).

